A Model of Muscle-Tendon Function in Human Walking

by

Ken Endo

Submitted to the Department of
Electrical Engineering and Computer Science
in partial fulfillment of the requirements for the degree of

Doctor of Philosophy

at the

MASSACHUSETTS INSTITUTE OF TECHNOLOGY

June 2012

Author .....
Department of
Electrical Engineering and Computer Science
May 23, 2012

Certified by .....
Hugh Herr
Associate Professor of Media Arts and Sciences
Thesis Supervisor

Accepted by .....
Professor Leslie A. Kolodziejski
Chairman, Department Committee on Graduate Theses

A Model of Muscle-Tendon Function in Human Walking

by

Ken Endo

Submitted to the Department of
Electrical Engineering and Computer Science
on May 23, 2012, in partial fulfillment of the
requirements for the degree of
Doctor of Philosophy

Abstract

In order to motivate the design of legged machines that walk as humans do, this thesis investigates how leg muscles and tendons work mechanically during level-ground human walking at self-selected speeds. I hypothesize that quasi- passive, series-elastic clutch units spanning the knee joint in a musculoskeletal arrangement can capture the dominant mechanical behaviors of the human knee in level-ground walking. As a preliminary evaluation of this hypothesis, I develop an under-actuated model of the human leg in walking where each muscle-tendon unit spanning the knee joint is represented as a simple linear spring in series with a clutch. I vary model parameters, or spring constants and clutch engagement times, using an optimization scheme that minimizes ankle and hip actuator work while still maintaining human-like knee mechanics. For model evaluation, kinetic and kinematic gait data are employed from nine participants walking across a level-ground surface at self-selected gait speeds. With this under-actuated leg model, I find good agreement between model quasi-passive knee torque and experimental knee values, suggesting that a knee actuator is not necessary for level-ground robotic ambulation at self-selected gait speeds.

As a further evaluation of the hypothesis of spring-like muscle-tendon behavior about the knee joint, a forward dynamics control scheme for the under-actuated model is developed. Hill-type muscle models are employed to model the ankle soleus and hip monoarticular muscles. Further, the model's series-elastic clutches are engaged with a simple state machine based on electromyography (EMG) data from the literature. Muscles are controlled with simple feedback controls representing the reflexive architecture of the human neuromuscular system. Following an optimization procedure, the model is shown to predict joint and muscle biomechanics, as well as the metabolism of walking humans, supporting the idea that muscle-tendon units spanning the human knee joint mainly operate as spring elements during neural activation, affording the relatively high metabolic walking economy of humans.

Thesis Supervisor: Hugh Herr
Title: Associate Professor of Media Arts and Sciences

Acknowledgments

This thesis is a culmination of many people's contributions. Much of the credit for this work belongs to those listed and unlisted who donated their valuable time and thought.

I would like to thank my thesis supervisor, Professor Hugh Herr, for his advice, support, guidance and friendship during my time at the Biomechatronics Group. I am a person who want to work broadly and he always supports me even outside of the laboratory.

I thank the members of my thesis committee: Prof. Russ Tedrake, Prof. Tomas Lozano-Perez for providing invaluable insight and guidance during the preparation of this thesis. Especially, I submitted my thesis draft only one day before the defense. I really appreciate for their flexibility. Here is another story about me and Russ. I met him back in 2005 for the first time in Japan, and he encouraged me to apply for MIT Ph.D. program and introduced Hugh to me. I would not be here without him.

I also want to offer thanks to those in the Biomechatronics Group with whom I have worked for making it such an exciting working environment. I thank Prof. Hartmut Geyer and Prof. Sungho Jo for help and advice on my simulation model. Thanks Bob Emerson, a prosthetist for finding patients for me and all alignment and advice. Thank Ernesto Martinez, Grant Elliott, and Michael Eilenberg for sharing a office with me. I really appreciate for their friendship and encouraging me when I felt much stress. Especially, Ernesto and Michael spent much time on assistant of my clinical study. Thank Jared Markowitz, Pavitra Krishnaswamy and Todd Farrell for useful conversation of neuromuscular model of human body. This conversation always directed me correctly. Thanks my smart UROP Nifer Fasman who contributed a lot to muscle energetics evaluation. Thank legend of biomech group, Prof. Marko Popovic, Waleed Farahat, Lee Magnusson, Bruce Deffenbaugh, Samuel Au, Goutam Reddy, Prof Conor Welsh and Jeff Weber for being a constant source for new ideas and feedbacks. Thanks Tesha Myers and Sarah Hunter for supporting biomech group as an administrative. Thanks to all of them and to everyone else who has worked in

the research group.

I also want to Thank members of Media lab. Prof. Hiroshi Ishii always inspired and encouraged me as a professional researcher as well as a japanese. Thank Joi Ito, a new director of Media lab for his advice on my new start-up. Thank Prof. Rosalind Picard, Prof. Sep Kamver and Frank Moss and all members in East lab for sharing our huge space and useful chatting.

Besides, I thank D-lab community including Amy Smith, Victor Gau Serrat, Joost Bonsen, Gwyndaf Jones, and Dennis Nagel. Especially I really appreciate Jose Gomez Marquez and Anna Young for friendship beyond D-lab community. Moreover, Thank Goutam Reddy, Todd Farrell, David Sengeh from Biomech group, Nadya Peek and Kenny Cheung from center for bits and atoms and Fablab team for teaming up with me on Developing World Prosthetics. Thanks Dr. Wu Yeongchi, Andew Hansen at Northwestern University, and Joel Sadler, a Ph.D. student at stanford universty for sharing project on appropriate orthopedic technology. My experience in D-lab was great and directed me to my current future plan. Thanks to all of D-lab members and to everyone else who has worked in the research group.

I thank all of the members in the Japanese Association of MIT for providing an excellent community for me that was supportive, friendly, and constructive for my growth.

I personally thank Kazuhiro Yoshikawa, my friend and above-knee amputee. When his cancer was found at this knee joint, he said he wanted to walk by himself rather than using assistive robot. This inspired me and drove me to apply for MIT.

Finally, My biggest appreciation goes to my dear family. My father past away in 2009. He always encouraged me to work harder. I thank for his huge love and my mother and brother for supporting my life here. And I, of course, thank my wife, Akiko and son, Kakeru. When I finished my defense, Tomas said Akiko is a Saint as Kakeru was 6 month old at that time. I think that's true. I cannot appreciate too much.

Contents

List of Figures

List of Tables

Chapter 1

Introduction

Bipedal walking is the human body's natural method for moving from one location to another and is usually the most convenient way to travel short distances. Bipedal walking uses a repetitious sequence of limb motions to move the body forward while maintaining stability. It is hypothesized that metabolic energy consumption is minimized in normal walking at the self-selected speed [48]. As walking is frequently and casually used to conduct daily activities, a disability of the lower extremities can dramatically reduce a person's quality of life (QOL). Conventional prosthetic and orthotic leg technology cannot fully emulate biological leg function in walking, leading to higher metabolic demand, slower walking speeds and problems of balance.

There are approximately 19 million Americans with physical ambulatory disabilities [58]. In particular, there are more than 1.8 million lower extremity amputees in the United States, while 134,000 people's legs are amputated every year [63]. These statistics data show high demand for prosthetic and orthopedic technologies, which are often used to restore lost motor function in individuals suffering from leg pathology. There are various kinds of commercial prosthetic and orthotic legs currently available, however, prosthetic leg or orthotic device is able to completely restore full intact leg function. One reason for this deficiency is that current actuator technology is not small and powerful enough to fit within the limited space and generate as much positive power as muscles for its mass. Another problem is battery weight causing an increase in walking metabolic cost. One great challenge in prosthetic and

orthotic design is to reduce electrical power usage and the metabolic cost for walking at self-selected speeds in persons with leg pathology. In order to do this, we need to understand how humans walk anatomically, physiologically and neuromechanically.

1.1 Human physiology and locomotion

The human body has approximately 640 muscles [52] that are used to interact with the external environment. Humans use muscles quite economically, particularly in walking. Such low metabolic cost is achieved by using the elasticity such as tendons in series with the actuation of the muscle fascicle. A key research challenge is to investigate how the elastic component and muscle fascicles in each muscle-tendon unit (MTU) behave during locomotion. Unfortunately, there does not yet exist an experimental methodology capable of detecting the state of all muscles and tendons at the same time.

1.1.1 Muscle state measurement

There are several methods to estimate muscle states from joint kinematics and anatomical data [19, 59, 49], using length change of MTUs measured in cadavers as functions in terms of ankle, knee, and hip joint angle. However, most approaches provide length changes of the whole MTU and thus do not allow one to examine the interaction of the contractile element and its tendon. This unknown aspect is investigated in a recent study using real-time ultrasonography, a scanning method that allows reliable and non-invasive measurements of intact human fascicular kinematics. Fukunaga et al. [55] presented in-vivo mechanical data of the fascicles and tendon of the ankle plantar flexor muscle, gastrocnemius medialis (GM) in walking using ultrasonography measurement technology. These data revealed that GM length stayed almost constant while the Achilles tendon was lengthened during the stance phase. Subsequently Ishikawa et al. [26] determined the length changes of GM, soleus, and their associated tendons during walking using a similar technique. Finally, Lichtwark and Wilson [16] presented the length changes of the muscle fascicle, tendon, and aponeu-

rosis in the GM MTU for walking and running. Since at least one sensor needs to be attached to the skin over a muscle and the measurement setup interferes with normal body motions, measuring all muscle states simultaneously is problematic.

1.1.2 Muscle state estimation

Instead of directly measuring muscle state, some researchers have attempted to estimate them from ground reaction forces (GRF) and joint kinematics. GRF and joint angles are captured with a force plate and motion capture system, respectively, and each joint torque is calculated through inverse dynamics. Using only net joint torque and state, calculating the state of each muscle is challenging, since the number of muscles is larger than the number of joints. To solve this problem, dynamic programming has been adopted. Anderson and Pandy [5] employed a three-dimensional human musculoskeletal model with Hill-type muscle models and optimized muscle activations to minimize metabolic cost. However their model prediction overestimates metabolic cost by 46%. In more recent work, Neptune et al. [42] used a two-dimensional human musculoskeletal model with a Hill-type muscle model and optimized muscle activations such that the error between the simulation result and kinetic and kinematic human gait data were minimized. Again their muscle fascicle mechanical work estimate was approximately twice as large as would be expected from metabolic measurements.

1.1.3 Muscle controller investigation

In order to restore full leg function in walking, mechanical MTU unit behavior: how each muscle is controlled as well as the interaction between elastic components and muscle fascicle needs to be better understood. Several empirical studies have demonstrated the importance of afferent feedback to the plantar flexors during stance in walking. These studies record the changes in muscle EMG signals when the gait of a subject is perturbed either by changing the inclination of the walking surface or by forcing muscle-tendon length changes using an orthosis. For example, Grey et al.

[18] demonstrated that the late stance phase soleus activity is most likely enhanced by force feedback. Subsequently, Klint et al. [3] investigated the contributions of afferent feedback at self-selected walking speed on different inclinations. They found that the muscle fascicle length-related feedback mediates force output during the stance phase. In later work, Klint et al. [4] isolated the contributions of force-based and length-based afferent feedback during different intervals in the stance phase at self-selected walking. They found that force feedback was dominant in late stance but contributed little in the mid stance phase, where length-based feedback is more dominant. Although these empirical studies are notable, these approaches are limited in the number of muscle they can focus on.

While these empirical approaches have shown qualitative comparison of force and muscle-tendon states, forward dynamics simulations have traditionally been used for the purpose of estimating muscle feedback architecture. Taga [53] proposed a noteworthy neuro-musculoskeletal model of biped walking with eight body segments and 20 muscles. The sequence uses inputs from neural oscillators located at the joints to generate stable limit cycles. The impedance controllers representing muscles are critical in the generation of gait through feedback. Further studies [54] demonstrated that the model generates robust walking motions against external perturbations or variations in terrain. From the perspective of neurophysiological modeling, the Taga model still lacks an explicit evaluation of its plausibility. It is currently unknown whether humans use such global states to generate walking. Another neuromechanical model by Ogihara and Yamazaki [43] emphasizes neural pattern generators (NPGs) and a neural feedback control system that consists of muscles, reflexes from muscle spindles, golgi tendon organs, and foot tactile receptors. A genetic algorithm optimizes the neural network weights by minimizing energy consumption per step. The neural control algorithm in this model is more complicated than Taga, and its walking performance is less robust. Contrary to a CPG based-controller, Jo [28] proposed a controller that comprises a scheduled cerebrocerebalar interaction, pulse-like feedforward commands, and segmental reflex modulation of muscular synergies. This model transitions from standing still to walking at 1.5m/s. Geyer and Herr [21], in distinction, developed a

model of human walking that is driven solely by muscle reflex behaviors that encode principles of legged mechanics. The model shows qualitative agreement with joint angles, joint torques and muscle activations, suggesting that human motor output could largely be shaped by muscle reflex behaviors. More recently, Song and Geyer [17] optimized their model such that the metabolic cost was minimized for different walking speed and showed the model can transition its walking speed by changing key parameters.

All these models are investigated with forward dynamics simulations and use predefined musculoskeletal models with model input parameters such as muscle maximum force and velocity, as well as tendon stiffness.

1.1.4 Joint kinematics and metabolic cost of transport of Human walking models

A number of researchers have attempted to develop musculoskeletal models for walking, and evaluated their metabolic cost of transport (COT) and joint kinematics. Figure 1-1 shows the cross-correlation coefficient of joint angle and metabolic COT of two musculoskeletal walking models. Geyer estimated the metabilic cost with Umberger's model [56], and Anderson and Pandy estimated it their own method. A cross-correlation coefficient is a quantity representing an agreement ($R = 1$ shows a perfect agreement), and metabolic COT is metabolic energy expenditure normalized by body weight and walking distant. The dashed line and shaded area are the average of human metabolic COT and one standard deviation from the average, respectively. The black square and circle are two musculoskeletal models (square: Geyer and Herr model [21], circle:Anderson and Pandy model [5]) which showed relatively low metabolic COT and high R values. However, none of researchers has ever developed a musculoskeletal model in the region of human metabolic COT with high R value.

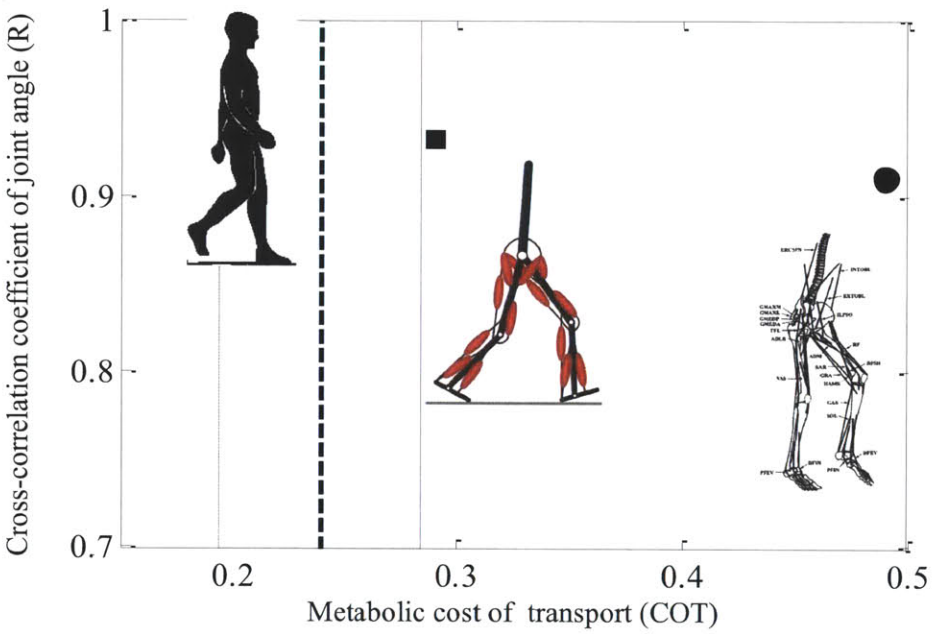

Figure 1-1: Current studies on musculoskeletal model for walking

The dashed line and shaded area are the average of human metabolic COT and one standard deviation of the average, respectively [24]. The black square and circle are two musculoskeletal models developed by [21, 51] and [5], respectively. Geyer estimated the metabilic cost with Umberger's model [56], and Anderson and Pandy estimated it with their own method.

1.2 Biped walking robots

	 ASIMO	 The Cornell Biped	 Human
Versatility	Moderate	Low	High
Energetic COT	2.8*	0.2	0.2

Table 1.1: Comparison of bipedal walking robots and human locomotion
*estimated from published resources

The human body is often compared with various types of biped walking robots. Table 1.1 shows comparison of human walking with that of two extreme examples of biped robots, ASIMO and the Cornell powered biped. ASIMO is one of the most advanced humanoid robots developed by HONDA [1], which can walk at $0.44 \sim 0.89$ m/s and can maintain balance while walking on uneven surfaces. ASIMO's energetic COT are estimated from published resources. Though ASIMO's walking behavior shows moderate versatility, its metabolic economy is extremely poor since ASIMO's joints are driven by electrical motors with harmonic drive gear heads. On the other hand, Collins and Ruina developed an energetically economical biped walking robot [9] based on passive dynamic walking [37], which requires only two actuators at the ankle joints. Although this robot can walk with quite low electrical and mechanical energy consumption, it can walk only at one walking speed (0.44 m/s) with less versatility than ASIMO.

1.3 Research objectives

Humans have even more versatility than ASIMO and walk with low energetic COT comparable to the Cornell biped. How do humans walk so economically? It is hypothesized that the morphology and control of the human leg allows for significant energy

exchange between the kinetic, gravitational and elastic energy domains throughout the walking cycle, thereby minimizing the required muscle fascicle work and metabolic COT. This particular hypothesis is difficult to evaluate since the elastic energy storage in elastic elements such as tendons during human walking cannot yet be measured experimentally. Computational simulations also fail to estimate a reasonable energetic economy for walking at self-selected speed. One possible cause is that such models optimize only muscle control parameters, with leg morphological parameters being held constant. The stiffness of the total series-elastic element is generally unknown. Since fascicle work is directly dependent on how much elastic energy is stored and released from the muscle-series compliant structures, it is possible that both the stiffness of the series-elastic element as well as muscle control parameters must be optimized simultaneously in order to obtain a reasonable estimation of elastic energy storage and muscle fascicle work. This thesis investigates such an optimization.

This thesis presents a two-dimensional musculoskeletal model that walks at human-like speeds with a human-like metabolic COT. Moreover, the model is in qualitative agreement with muscle electromyographic data (EMG), and joint mechanical data.

1.4 Thesis outline

In the chapter 2, a two dimensional musculoskeletal structure for a self-selected walking speed is proposed. Series elastic clutches and a minimal number of actuators are used in the model. In the chapter 3, as a further evaluation of the model, a control scheme for the actuators and in the musculoskeletal model is constructed with a forward dynamics simulation. Finally, conclusion and future work are stated in the Chapter 4.

Chapter 2

Musculoskeletal model optimization

The elasticity of MTUs plays an important role in reducing the walking metabolic COT. It may be suggested that quasi-passive series-elastic clutch (SEC) units spanning the knee joint in a musculoskeletal arrangement can capture the dominant mechanical behaviors in level-ground walking. As a preliminary evaluation of this hypothesis, a musculoskeletal model with SECs and the minimum number of series-elastic actuators (SEA) is constructed. Model parameters (spring constants and clutch engagement times) are then varied using an optimization scheme that minimizes ankle and hip actuator positive mechanical work while still maintaining human-like knee mechanics. Kinetic and kinematic gait data from nine participants walking across level ground at self-selected speeds are used to evaluate the model.

2.1 Method

2.1.1 Leg model

A number of research groups have worked on a human musculoskeletal model for self-selected walking, and none has yet achieved both human walking economy and biomechanics simultaneously. However, both human walking economy and biome-

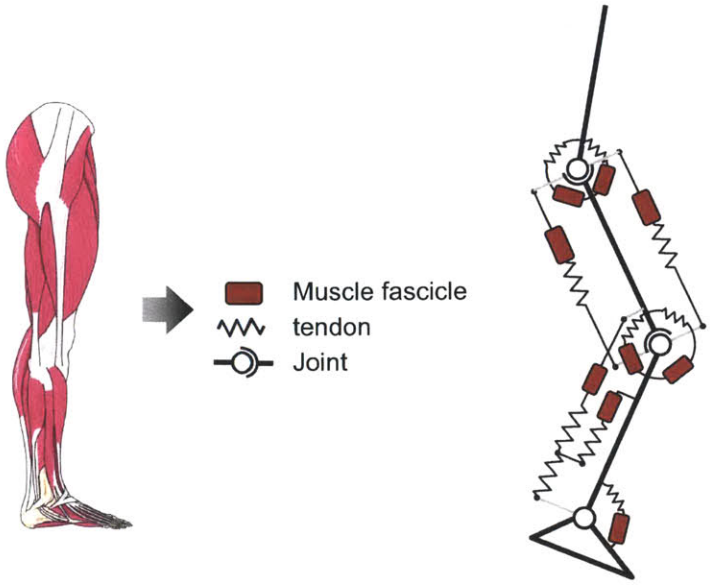

Figure 2-1: Human model with muscle-tendon units
Nine muscle fascicle and tendon units are attached to one leg. A muscle fascicle and tendon unit includes a contractile element and series elastic element as a tendon. Usually, A boundary and contractile element and series elastic element is unclear. Only achilles tendon is represented as a spring because, it boundry is obvious.

chanics are necessary to design assistive technologies which fully restore leg function. In order to satisfy these two requirements, a key approach here is to understand how humans use their muscles fascicles and series elasticities.

Commonly, a human walking leg is modeled in a two-dimensional saggital plane with dominant muscle groups atatched around ankle, knee and hip joint as shown in Figure 2-1. In this model, nine muscle fascicle and tendon units are attached per leg. A muscle fascicle and tendon unit includes a contractile element and series elastic element as a tendon. Usually, A boundary and contractile element and series elastic element is unclear. Only achilles tendon is represented as a spring because its boundry is obvious. Traditionaly, a computational muscle model such as Hill-type muscle model and bilinear model has been employed, which needs a large number of parameters. These models also need precise physiolosical parameters such as tendon stiffness, maximam contraction force, optimal muscle fiber length etc, and these numbers are usually difficult to be measured accurately due to the limitation of currenty

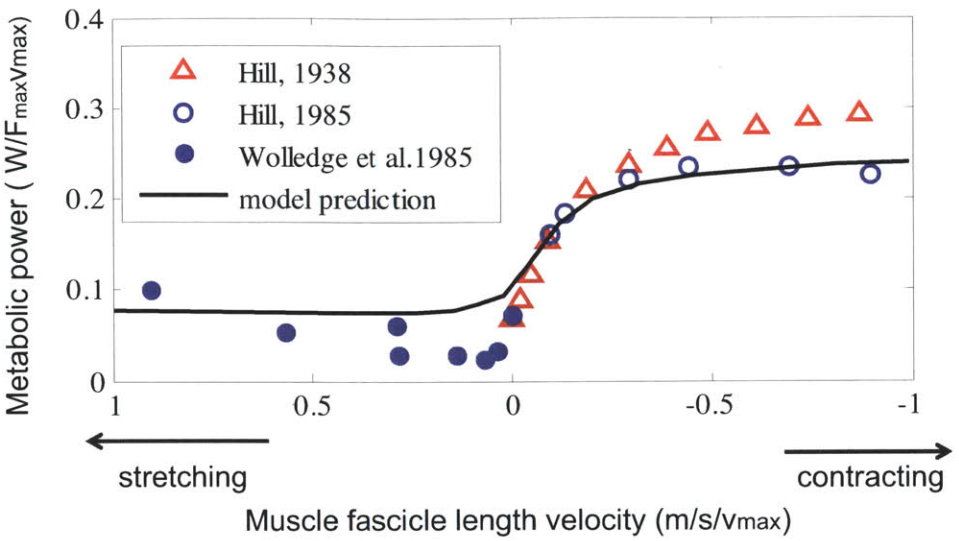

Figure 2-2: Muscle metabolic power in steady-state
Comparison of the steady-state rate of chemical energy liberation predicted the energetics model with experimental measurement, for frog sartorius at 0 deg. [34] Data for shortening is based on heat and work measurement of Hill. Data for stretch based on ATP hydrolysis measurement from several source (collected by Woledge et al.).

available measurement apparatus. In this research project, a muscle-tendon unit is modeled in simple way with based on several hypotheses in the following section.

Background and Hypotheses

Muscle energetics are quite unique. Figure 2-2 shows the relationship between muscle metabolic power and velocity [34]. These data were collected by measuring heat and work production for contraction, and ATP hydrolysis for stretch. Muscle metabolic power and velocity are normalized by maximum contraction force and maximum velocity of the muscle, and the maximum velocity, respectively. When a muscle is stretching (eccentric: $v > 0$) or isometric($v = 0$), metabolic power is relatively low. However, once a muscle starts to contract (concentric: $v < 0$), metabolic power increases sharply. This suggests that humans may minimize metabolic energy usage by keeping the fascicle velocity zero or even negative.

More recent reports also support this idea. For example, Ishikawa et al. [26] reports the length change of the soleus and gastrocnemius with in-vivo measurement

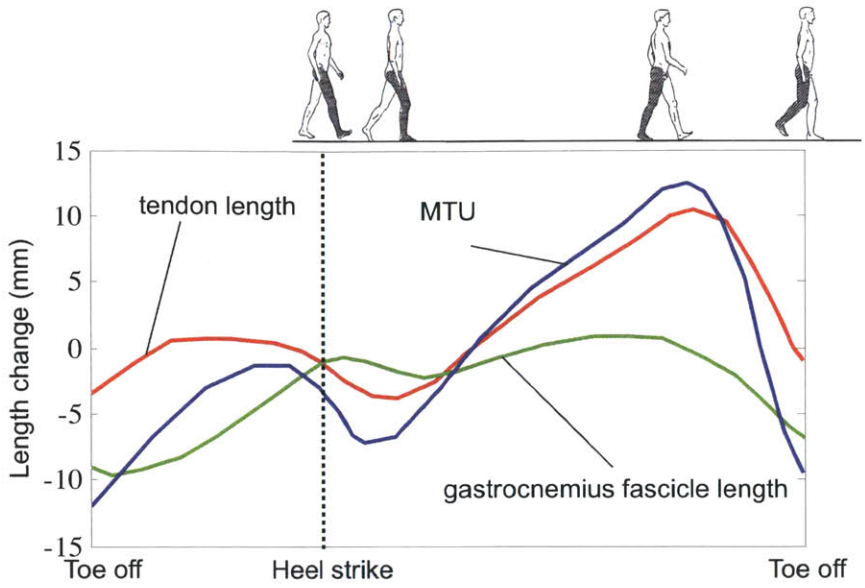

Figure 2-3: Length change of Gastrocnemius fascicle, tendon and MTU
An ultrasonographic apparatus was used to measure fascicle length in the medial gastrocnemius and soleus muscles during walking from eight male participants (28.4 yr, height 171.8 cm, mass 71.7 kg, self-selected walking speed 1.4 m/s) [26]. The length of gastrocnemius does not change from 30 % to 50 % of gait cycle, though the ankle and knee angles do change. This indicates the Achilles tendon is lengthened or shortened instead of the muscle fascicle.

as shown in Figure 2-3. An ultrasonographic apparatus was used to measure fascicle length in the medial gastrocnemius and soleus muscles during walking from eight male participants (28.4 yr, height 171.8 cm, mass 71.7 kg, self-selected walking speed 1.4 m/s). The length of gastrocnemius does not change from 30 % to 50 % of gait cycle, though the ankle and knee angles do change. This indicates the Achilles tendon is lengthened or shortened instead of the muscle fascicle.

Finally, Figure 2-4 shows knee joint net power during one gait cycle. Total net work at the knee joint is -5J with significant negative work during the swing phase. Historically, a spring-damper system or variable damper has been used for commercial prosthetic knee joints for this reason. However, a damper is a component which throws mechanical energy away as heat, and cannot reuse the energy again. Instead of dissipating mechanical energy, the body stores it in elastic storage, transfers it to the other joints and then reuse there.

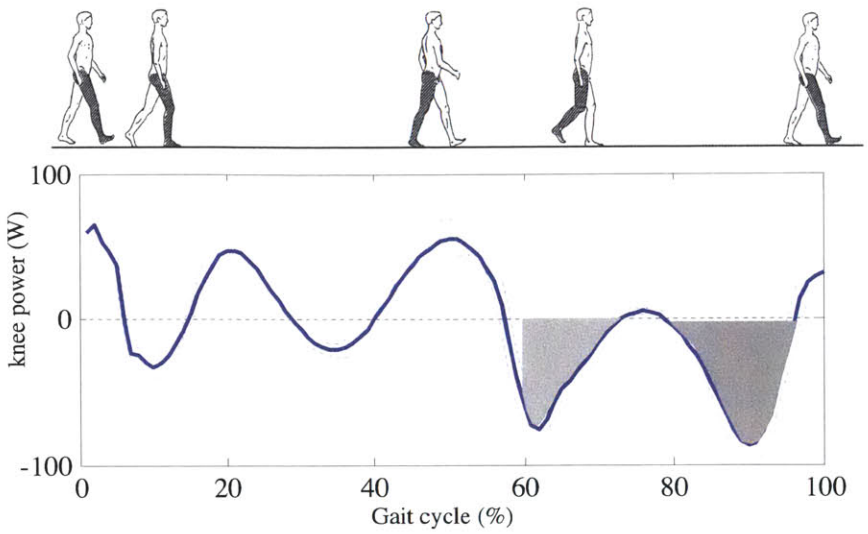

Figure 2-4: Knee joint mechanical power
Knee joint power is shown from a heel strike to the next heel strike of gait cycle. A subject is 81.9kg, 28yrs and walks at 1.27m/s as self-selected walking speed. Solid curve is the average of seven trials. The dotted curves are from one standard deviation from the average and shaded area indicates negative part of joint power during the swing phase. The data are from [23]

In summary, it is hypothesized that

- quasi-passive, SEC units spanning the knee joint in a musculoskeletal arrangement can capture the dominant mechanical behaviors of the human knee in level-ground walking,

- since an SEC is incapable of dissipating mechanical energy as heat, a corollary to this hypothesis is that such a quasi-passive robotic knee would necessarily have to transfer energy via elastic biarticular mechanisms to hip and/or ankle joints, and

- such a transfer of energy would reduce the necessary actuator work to track human torque profiles at the hip and ankle, improving the mechanical economy of a human-like walking robot.

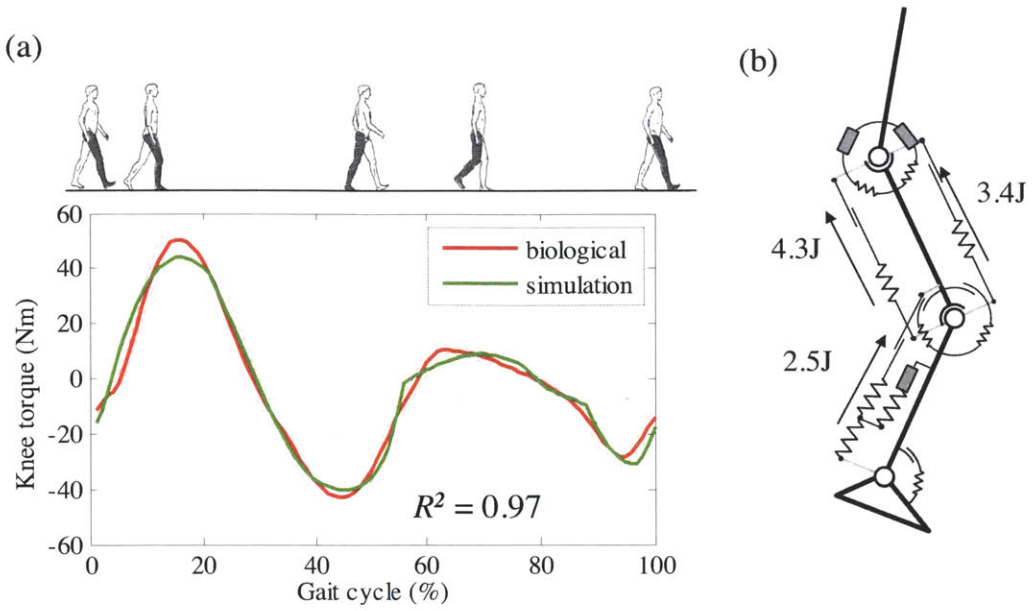

Figure 2-6: Knee torque agreement and energy transfer across joints
(a). Knee torque for one representative study participant (Participant 1 in Table A.1). The red curve is the mean of the inverse dynamics estimate of biological joint torque (n= 6 walking trials), and dashed lines are one standard deviation about the mean. The green curve is the model output. All curves start at heel strike (0% gait cycle) and end with the heel strike of the same leg (100% gait cycle). R^2 is calculated between biological data and simulation result. (b) Energy exchanges across joints. 3.4J and 4.3J are transferred from knee to hip joints though knee-hip anterior and posterior, respectively. Regarding to the ankle-knee posterior unit, energy goes back and forth between the upper and lower springs per one gait cycle, due to the ankle plantar flexor actuation. 2.5J is transferred from knee to ankle posterior.

2.2.2 Energy transfer across joints

Figure 2-6 (b) depicts energy transferred through biarticular units. As a biarticular unit spans multiple joints, mechanical energy can be carried from one joint to another: energy stored in the spring at one joint can be released at the other joint. The knee-hip anterior and posterior springs transferred 3.4 joules and 4.3J from the knee to hip joint, while the ankle-knee posterior unit transferred 2.5 J. Net mechanical works of participant 1 at ankle and hip joints for self-selected walking are 16.5J and 16.9J respectively, and -6.2J for knee joint. These numbers imply that energy absorbed at the knee joint is reused at the hip joint, and both knee-hip anterior and posterior units

Among the model's torque producing elements are six SECs. Each consists of a clutch in series with a spring, modeling a MTU operating elastically upon neural activation. Some are connected across a single joint (monoarticular) and others across two joints (biarticular). While a clutch is disengaged, the associated joint rotates without any resistance from the spring. When a clutch engages, the equilibrium position of the spring is thereby established, and any further rotation of the joint deflects the spring, producing torque about the joint proportional to the displacement from that equilibrium position. Energy is also stored in the spring as it is rotated away from its equilibrium position. Once a clutch has engaged, it remains engaged until joint rotation returns the spring back to its equilibrium position, at which point the clutch disengages; thus all energy stored in the spring is returned to the system before disengagement. It is assumed the SECs engage and disengage exactly once during a gait cycle.

In the model, the operation of these SECs is characterized by two parameters: the engagement point of the clutch, which sets the equilibrium position of the spring, and the spring constant. The spring constant is taken to represent the elasticity of the tendon, aponeurosis, surrounding tissue fascicles, and the elasticity of the muscle, potentially including any component of muscle elasticity produced by the neural reflex mechanisms of the muscle. It is difficult to further identify these subcomponents of elasticity due to the limitations of measurement technology and the complexity of the human body.

The engagement point parameter will be given as the point in time during a gait cycle when the clutch engages. I will describe this engagement point time parameter as a percentage of the gait cycle. SEC mechanisms cannot perform net work; they act only to store and then later release energy. In the calculations of the energetic cost of walking, I will assume zero energy is required to operate the clutched spring mechanisms. This approximates the comparatively small energetic cost of muscles operating isometrically.

It is well established that the net work of the knee joint in one gait cycle is negative while that of the ankle and hip joints are positive [61, 27]. This motivates the idea

that at self-selected walking speed, power generating force sources are required only at the hip and ankle joints. Three SEAs are included in the present model to provide this power requirement: two at the hip joint acting as an agonist-antagonist pair, and a single SEA at the ankle joint.

Each SEA consists of a power producing force source element in series with a linear spring, modeling a moving muscle and associated tendon. The SEAs are considered capable of producing any desired torque, but their output is only permitted to be unidirectional; they may act only in tension and never in compression. In calculating the energetic cost of operating the three SEAs, only the net positive power of the SEA's motor element, thus approximating the small metabolic cost of eccentric muscle work as zero. The sole model parameters characterizing these three SEAs are their spring constants.

If the force source element of an SEA were capable of both efficiently producing and absorbing work, the value of the spring constant would have no effect on the energetic cost of any cyclic operation. It is only because of the asymmetry in the metabolic cost of eccentric and concentric muscle work [34] that the determination of the spring constant (and the associated tendon elasticity) is of interest.

A further rotational elastic element is provided at the hip to emulate hip ligament. This is a passive, unidirectional rotary spring with a fixed engagement angle providing torque as the hip rotates past that angle. It is parameterized in the model by its engagement angle and its spring constant.

An additional passive spring spans the ankle joint, modeling the Achilles tendon. Its distal end connects directly to the foot segment and its proximal end is connected to both an SEC (modeling the gastrocnemius) and an SEA (modeling the soleus). This spring is characterized by a fixed rest length and linear spring constant taken from literature [36].

All monoarticular components of the model are considered rotary, and their spring elements are described by rotary spring rates (torque per angle) and their engagement point is a joint angle, or equivalently, the point in time during the gait cycle at which that joint angle is attained.

For biarticular springs, moment arms for each joint are taken from literature [39, 35], and the spring is linear with its associated clutch engagement point defining its rest length. The joint torques for the two joints of a biarticular springs are given by the calculation:

$$F(t) = k\{R_1(\theta_1(t) - \theta_1(t_0)) + R_2(\theta_2(t) - \theta_2(t_0))\} \quad (2.1)$$

$$\tau_1(t) = -R_1 F(t) \quad (2.2)$$

$$\tau_2(t) = -R_2 F(t) \quad (2.3)$$

where $F(t)$ is the force in the biarticular spring at time t, k is the spring constant of the biarticular spring, R_1 and R_2 are the moment arms of the two joints, $\theta_1(t)$ and $\theta_2(t)$ are the joint angles of the two joints at time t, t_0 is the engagement time of the biarticular clutch, and $\theta_1(t)$ and $\theta_2(t)$ are the resulting joint torques at the two joints at time t.

2.1.3 Optimization strategy

The eleven torque producing elements of the model: six SECs, three SEAs, one hip ligament spring, and the Achilles tendon spring, are characterized by a total of nineteen parameters. I next describe a series of procedures for determining the set of values of these parameters which produce the best match between the model's dynamic behavior and the experimental subjects' observed walking behavior while at the same time minimizing the energetic cost of walking.

Biomechanical data was obtained for nine participants using a VICON motion capture system and two force plates. Sagittal plane data were extracted for joint angles, torques, and powers for the hip, knee and ankle. The data collection and participant characteristics are fully described in the Appendix A. The two parameters for the Achilles tendon are its rest length and spring constant. These are taken from literature [36] and scaled to the individual subject as follows:

$$k_{Achilles} = \frac{Y \times CSA}{l_{Achilles}} \tag{2.4}$$

where Y is the Young's modulus of the tendon, CSA is its cross sectional area, and $l_{Achilles}$ is the lower Achilles tendon length which is also scaled to the subject's height. Knowing these values, the moment arm of the tendon's distal end attachment to the foot segment, and the measured ankle plantar flexor torque, the length of this spring and the spring force throughout the gait cycle is determined. This immediately gives the position and force at the proximal end of this Achilles tendon spring. Since the ankle-knee posterior SEC and the ankle plantar flexor SEA are joined to the proximal end of the Achilles tendon spring, they must match this motion, and their combined forces must exactly counter the force of the Achilles tendon spring. Dorsiflexion torque at the ankle is entirely produced by the dorsiflexor SEC. The engagement time and spring constant of this are determined by least squares fitting to the experimental dorsiflexion ankle torque. Since no other element spanning the ankle joint is capable of producing dorsiflexion torque, the action of this clutched spring is independent of the rest of the model, and does not affect the determination of the other model parameters.

The model's remaining five SECs all span the knee joint, and their parameters are determined by least squares fitting the sum of their torques to the experimental knee torque for the period of a full gait cycle. A two-step optimization procedure using a genetic algorithm followed by a gradient descent search is utilized for this fitting. The genetic algorithm is used to overcome the existence of local minima. The gradient descent method refines the solution once the region of the global minimum is identified. Bounds for the genetic algorithm search space must be provided, and these were based on qualitative electromyographic (EMG) data from literature [61] for the major anatomical correspondents of the actuators. The search regions for the engagement time parameters are set to be significantly larger than the periods of EMG activity, as EMG activity is not synchronous with muscle activation time. Bounds on the spring constant parameters were also provided by examining the maximum

torque occurring within the engagement time periods' bounds.

Once the parameters of the five SECs spanning the knee joint are found, their contributions to the torque at the hip are known. The two hip SEAs and hip ligament spring must then provide any additional torque necessary to exactly match the experimentally measured hip torque. The model parameters for these three units are selected to minimize the net positive work performed by them during a full gait cycle. In particular, this is the net positive work (concentric work) of the motor elements of the two SEAs at the hip.

The hip ligament spring is a passive element and cannot provide energy, however, if properly parameterized, it does act to reduce the net positive work performed by the SEAs. To solve this optimization problem, I again use the genetic algorithm followed by gradient descent. This solution yields the spring constants of the two SEAs at the hip and the spring constant and engagement angle of the hip ligament spring.

The sole remaining model parameter to be determined is the spring constant of the ankle plantar flexor SEA. This SEA acts in parallel with the gastrocnemius SEC to produce the force in the Achilles tendon spring. Since the forces in the Achilles tendon spring and the ankle-knee posterior spring are already known for the entire gait cycle, I know what force the ankle planarflexor SEA must produce. What I seek is the spring constant for this SEA which minimizes its net positive work during the production of this force. Once again, the optimal value is found with a genetic algorithm followed by gradient descent search.

2.1.4 Model evaluation

Model joint torque agreement

To evaluate the level of agreement between experimental data and optimization results, I used the coefficient of determination, R^2, where $R^2 = 1$ only if there is a perfect fit and $R^2 = 0$ indicates that the model's estimate is no better than using the mean experimental value as an estimate. More specifically,R^2 was defined as:

$$R^2 = 1 - \frac{\sum_{i=1}^{100}(x_i^{bio} - x_i^{sim})^2}{\sum_{i=1}^{100}(x_i^{bio} - \bar{x}^{bio})^2} \tag{2.5}$$

where x_i^{bio} and x_i^{sim} are the biological and model data at the ith percentage gait cycle. $\bar{x}^{bio}$ is the grand mean over all walking trials and gait percentage times analyzed, or:

$$\bar{x}_{bio} = \frac{1}{N_{data}N_{trial}} \sum_{i=1}^{N_{trial}} \sum_{j=1}^{N_{data}} x_{ij}^{bio} \tag{2.6}$$

where N_{data} and N_{trial} are the numbers of data points and trials, respectively.

Energy transfer across joints

As the model has biarticular units, stored energy at one spring from one joint could be released to the other joint. The energy transfer, for instance, from joint 1 to joint 2 would be calculated as follows:

$$ET_{1-2} = \frac{W_2 - W_1}{MgL_{leg}} \tag{2.7}$$

where W_1 and W_2 are total net work done by biarticular unit at joint 2 and 1, respectively. This value is dimensionless, normalized by body weight and leg length of the participants.

Mechanical cost of transport

A key issue in locomotion is energy usage. The mechanical COT of level ground self-selected walking c_{mt} [9] is defined as follows:

$$c_{mt} = \frac{W_{act}^+}{MgD} \tag{2.8}$$

where W_{act}^+ is positive mechanical work done by the three force sources. This is a dimensionless number normalized by body mass, Mg and walking distance, D.

Whole-body mechanical energetics

Willems et al. [60] reported the total energy level of the whole body subdivided into n rigid segments can be measured from the gravitational potential energy and the kinetic energy of each segment. However, as Ishikawa et al. [26] showed, the elastic element in muscle tendon units stores a considerable amount of energy. This indicates that elastic energy storage must also be considered as another domain of whole body energetics. As our model includes elastic elements, the total whole body energy $E_{tot,wb}$ can be calculated from the gravitational potential energy E_{pot}, the kinetic energy E_k and elastic energy storage E_e as follows:

$$E_{tot,wb} = E_{pot} + E_k + E_e \tag{2.9}$$

$$= Mgh_{cm} + \frac{1}{2}Mv_{cm}^2 + \sum_{i=1}^{n}(\frac{1}{2}m_i v_{r,i}^2 + \frac{1}{2}m_i K_i^2 w_i^2) + \frac{1}{2}\sum_{i=1}^{11} k_i \Delta x_i^2 \tag{2.10}$$

where, h_{cm} and v_{cm} are the height and the linear velocity of the center of mass of whole body, $v_{r,i}$ is the linear velocity of the center of mass of the ith segment relative to the center of mass of whole body, w_i and K_i are the angular velocity and the radius of gyration of the ith segment around it's center of mass, g is the acceleration due to gravity, k_i and Δx_i are the spring coefficient and displacement of ith spring. h_{cm} and v_{cm} are calculated from the position of center of mass. The position of the center of mass of the whole body is calculated from the VICON system captured data as follows:

$$\vec{r}_{cm} = \frac{1}{M}\sum_{i=1}^{n} M_r^i \vec{r}_{cm}^{\,i} \tag{2.11}$$

where $\vec{r}_{cm}$ is the vector to the CM of the whole body, M_r^i is mass of ith segment and is the vector to the CM of ith segment relative to the CM of whole body. h_{cm} is the vertical element of $\vec{r}_{cm}$ and v_{cm} is obtained as the Euclidean norm of the derivative of $\vec{r}_{cm}$. Cavagna et al. [8] reported the mechanical energy exchange of the body's center of mass (potential and kinetic energy of the CM) during normal walking, but

did not consider elastic energy storage within the muscle-tendon units. The model enables an estimate of elastic energy storage and the percentage recovery between elastic energy and potential/kinetic energies of the body in walking. The percentage recovery ($\%REC$) between elastic energy and potential/kinetic energy is defined as follows:

$$\%REC = \frac{|W_{pk}| + |W_e| - |W_{tot}|}{|W_{pk}| + |W_e|} \tag{2.12}$$

where W_{pk} is the sum of the positive increments of potential/kinetic energy, W_e is the sum of the positive increments of elastic energy, and W_{tot} is the sum of positive increments of both curves in one complete walking cycle. The percentage recovery is 100 percent when the two energy curves are exactly equal in shape and amplitude, but opposite in sign. In that case, the total mechanical energy of the body does not vary in time. Finally, I calculated total net actuator work (ActNet), positive series-spring work (ElaPos, elastic energy recovered from the series-spring), negative actuator work (ActNeg) and positive actuator work (ActPos) [42].

2.2 Results

2.2.1 Model knee torque agreement with biological data

Figure 2-6 (a) shows the biological and model simulated torques of the knee joint for one representative study participant (participant 1 in Table A.1). Hip and ankle joint torque agreement are not illustrated, as the SEAs are controlled to generate the experimentally observed hip and ankle plantar flexion torques. From Figure 2-6 (a), it is seen that the model's simulated torque curves agree well with biological data at the knee joint, as $R^2 = 0.97$. Moreover, as Table 2.2.1 shows, the R^2 value for knee joint torque for all nine participants is 0.95 ± 0.03. These numbers indicate the quasi-passive elements can capture the dominant knee behavior, even though no power producing actuator spanned that joint.

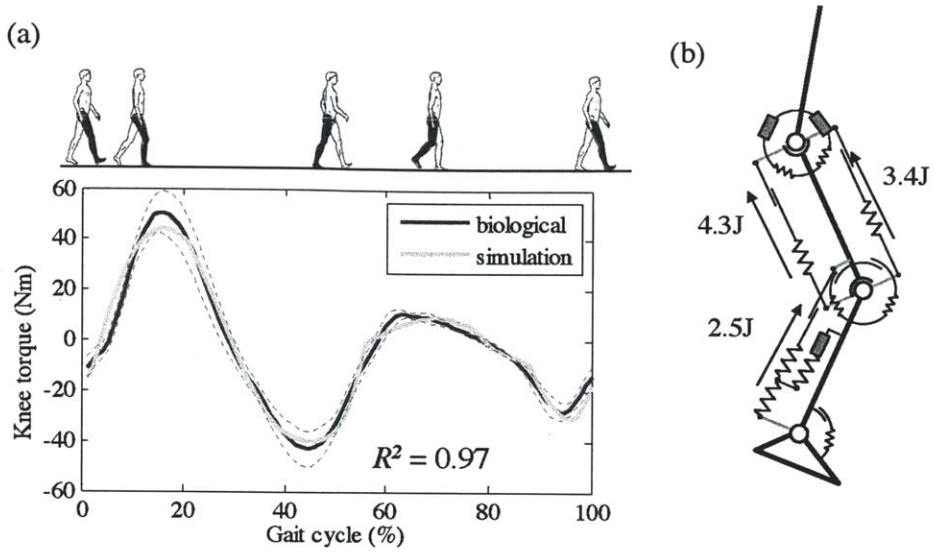

Figure 2-6: Knee torque agreement and energy transfer across joints
(a). Knee torque for one representative study participant (Participant 1 in Table A.1). The red curve is the mean of the inverse dynamics estimate of biological joint torque (n= 6 walking trials), and dashed lines are one standard deviation about the mean. The green curve is the model output. All curves start at heel strike (0% gait cycle) and end with the heel strike of the same leg (100% gait cycle). R^2 is calculated between biological data and simulation result. (b) Energy exchanges across joints. 3.4J and 4.3J are transferred from knee to hip joints though knee-hip anterior and posterior, respectively. Regarding to the ankle-knee posterior unit, energy goes back and forth between the upper and lower springs per one gait cycle, due to the ankle plantar flexor actuation. 2.5J is transferred from knee to ankle posterior.

2.2.2 Energy transfer across joints

Figure 2-6 (b) depicts energy transferred through biarticular units. As a biarticular unit spans multiple joints, mechanical energy can be carried from one joint to another: energy stored in the spring at one joint can be released at the other joint. The knee-hip anterior and posterior springs transferred 3.4 joules and 4.3J from the knee to hip joint, while the ankle-knee posterior unit transferred 2.5 J. Net mechanical works of participant 1 at ankle and hip joints for self-selected walking are 16.5J and 16.9J respectively, and -6.2J for knee joint. These numbers imply that energy absorbed at the knee joint is reused at the hip joint, and both knee-hip anterior and posterior units

	R_k^2	c_{mt}	ET_{k-h}	ET_{a-k}	%REC(%)	Actnet	ActPos	ActNeg	ElaPos
1	0.97	0.04	0.010	0.004	76.8	0.024	0.035	-0.010	0.051
2	0.95	0.04	0.024	0.008	85.5	0.005	0.025	-0.020	0.062
3	0.97	0.03	0.028	0.006	78.5	0.006	0.021	-0.015	0.067
4	0.97	0.06	0.014	0.014	73.1	0.030	0.046	-0.015	0.066
5	0.96	0.05	0.031	0.008	81.5	0.003	0.040	-0.037	0.064
6	0.91	0.04	0.029	0.005	81.1	-0.004	0.028	-0.031	0.052
7	0.98	0.02	0.019	0.003	79.9	-0.009	0.018	-0.027	0.061
8	0.96	0.06	0.027	0.003	67.2	0.028	0.046	-0.018	0.059
9	0.96	0.05	0.036	0.003	83.1	-0.014	0.048	-0.062	0.078
mean	0.96	0.04	0.024	0.006	78.6	0.008	0.034	-0.026	0.063
s.d.	0.02	0.01	0.008	0.004	5.6	0.002	0.012	0.016	0.081

Table 2.1: Simulation results
R^2 of knee torque (R_k^2), mechanical COT (c_{cm}), total energy transfer from knee to hip (ET_{k-h}) and from knee to ankle (ET_{a-k}), percentage recovery ($\%REC$), net actuator work (ActNet), positive actuator work (ActPos), negative actuator work (ActNeg), positive spring work (ElaPos). Values listed for 9 study participants. All energy quantities are normalized by the product of leg length and body weight, except for the mechanical COT which is normalized by the product of stride length and body weight.

play an important role to carry that energy. In particular, the knee-hip biarticular unit is critical for both knee torque agreement and for minimizing the hip actuator usage.

Table 2.2.1 shows normalized energy transfer from knee to hip (ET_{k-h}), and ankle to knee (ET_{a-k}), which are made dimensionless by normalizing by body weight and leg length. As with participant 1, the other participants also show large amounts of energy transferred from the knee to the hip joint, while a smaller amount of energy is transferred from the ankle to knee joint.

2.2.3 Mechanical cost of transport

Table 2.2.1 shows the mechanical COT of walking as predicted by the leg model. The mechanical economy of nine participants is 0.04 ± 0.01. The mechanical COT of human walking has been estimated at 0.05 [Donelan et al. 2002], which is comparable with the average of the model. However, Donelan and his colleague calculated the

mechanical COT from GRF, which includes contribution of elasticity components and internal mechanical work as well as fource sources. This is discussed in the next chapter with consideration of dynamics.

2.2.4 Whole-body mechanical energetics

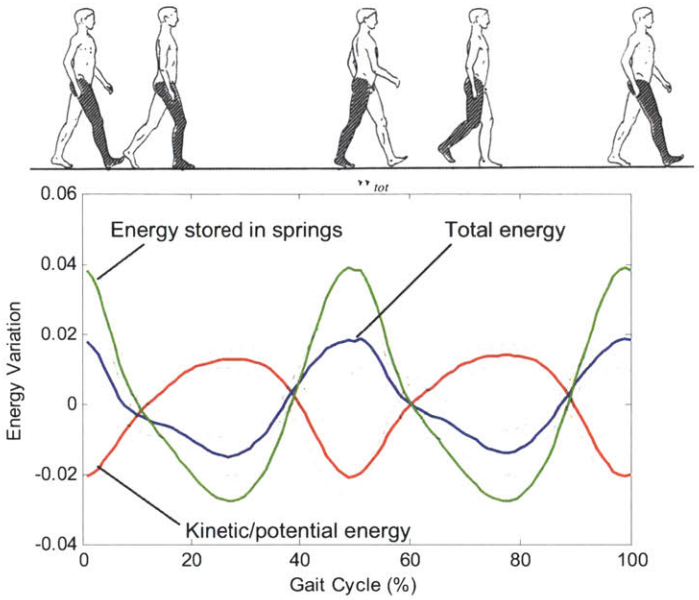

Figure 2-7: Potential, kinetic and elastic energy variation
Energy is dimensionless normalized by body mass and center of mass height. The red solid curve denotes energy which includes potential and kinetic energy at the center of mass as well as kinetic energy at the segments relative to the center of mass. The green curve is elastic potential energy stored in springs. The blue curve is total energy in the model. Each dotted line is one standard deviation from the solid line.

Figure 2-7 shows the average of nine participants' potential and kinetic energy variations in time during human walking, as well as variations in elastic energy storage from both legs as estimated by the model. These are dimensionless values normalized by body weight and CM height. The red and green curves are total energy stored by all elastic elements in the model and the sum of potential and kinetic energy of the body, respectively, and the blue curve is the sum of these two energy curves. The dotted curves are one standard deviation from the original data. Kinetic/potential and elastic energy are visibly out of phase implying that energy exchange occurs between

these mechanical energy forms, which is also shown in the previous optimization. The energy recovery between elastic energy and potential/kinetic energy is 78.6 ± 5.6 % as predicted from the leg model. Table 2.2.1 also shows total net actuator work (ActNet), positive actuator work (ActPos), negative actuator work (ActNeg), total positive spring work (ElaPos) for the nine participants of Table A.1. ActNet, ActPos, ActNeg, and ElaPos are made dimensionless by normalizing by body weight and leg length. These values are useful for comparing the mechanical work done by actuators and elastic elements. ActPos exhibits a large variance across experimental participants, possibly due to varying stabilization requirements of the upper body.

2.2.5 Model series-elastic unit activations

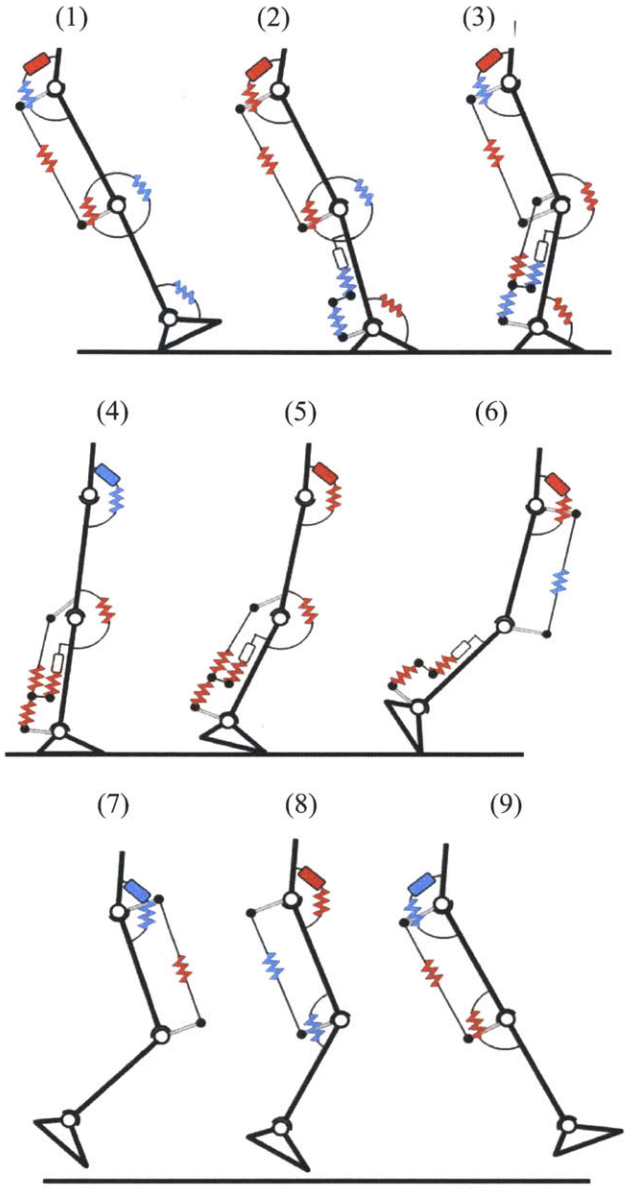

Figure 2-8: Walking sequence for one representative study participant
Walking sequence for one representative study participant (M = 81.9 kg) with clutch engagement and actuator activation. The spring is shown, when its associated clutch is engaged or actuator is activated. Otherwise, unit is not shown in the figure. Blue and red springs indicate storing or releasing elastic energy, respectively, and blue and red actuators perform negative and positive mechanical work, respectively. From (1) to (6), the leg is in contact with the ground, or stance phase, and from (7) to (9), the leg is apart from the ground or the swing phase. (1) heel strike (0%) (2) foot flat (10%) (3) knee maximum flexion in the stance phase (40%) (4) knee maximum extension in the stance phase (47%) (5) pre-swing (55%) (6) toe off (62%) (7) maximum knee flexion in the swing phase(70%) (8) (85%) (9) knee maximum extension in swing phase (96%).

Figure 2-8 shows the walking sequence with clutch engagement and actuator activity from the optimization results for participant 1. The spring is shown in each figure when its associated clutch is engaged or its actuator generates force. Otherwise, the unit is not shown in the figure. Blue and red springs indicate they are storing or releasing elastic energy, respectively. Regarding the actuators, blue and red actuators are performing negative and positive mechanical work, respectively. From (1) to (6), the leg is in contact with the ground (in stance phase), and from (7) to (9), the leg is off the ground (in swing phase). Each of the clutches and actuators seems to engage or activate according to ankle or knee behaviors. For example, at heel strike (1), the ankle dorsiflexor is engaged and its associated spring starts to store energy, and it continues to be engaged until the spring releases the energy. At foot flat (2), the ankle plantar flexor is activated, and the ankle-knee posterior clutch is engaged at maximum knee flexion (3). The knee-hip anterior is engaged just before toe off (5). The knee flexor and knee-hip posterior are engaged just before the knee extension of swing phase, which is between (8) and (9). This indicates that each unit may be controlled by the body-environment interaction using local feedback such as a reflex mechanism rather than high-level neural system.

The model was derived by inspection of the human musculoskeletal structure, and it is of interest to compare each muscle electromyography (EMG) with each spring-clutch, damper or actuator unit contribution, notwithstanding the fact that loose search limits for the genetic algorithm optimizations were based on qualitative EMG signals taken from the literature. Figures 2-9 (a), (b), and (c) show average power curves of the nine participants for each unit along with corresponding muscle EMGs from the literature [Perry 1992]. At the ankle joint, in Figure 2-9 (a), the tibialis anterior (TA), gastrocnemius (GAS) and soleus (SOL) generate the torque. TA is activated at the early stance phase to impede ankle plantar flexion, and GAS and SOL work from the mid stance phase to terminal stance to actively plantar flex the ankle. This is the same behavior exhibited by the ankle dorsiflexor and the ankle-knee biarticular unit in the model.

As Figure 2-9 (b) shows, the vastus muscle (VAS), gastrocnemius (GAS), bicep

femoris short head (BFsh), rectus femoris (RF) and hamstrings (HAM) are attached at the knee joint. VAS operates as a monoarticular knee extensor during the early stance phase. In human walking, the knee flexes just after heel strike. The VAS muscle performs work during that period of stance and generates torque to extend the knee. The knee extensor in the model acts in a similar manner to the VAS. The GAS is a flexor for the knee joint and it is activated at mid stance phase. After knee flexion during the stance phase, the human knee extends and then flexes again in preparation for toe off. The GAS works to flex the knee at the mid stance phase. The human leg also has a monoarticular knee flexor, namely the BFsh. The BFsh flexes the knee joint at the terminal swing phase and the early stance phase. The model's knee flexor performs a similar function.

In the model, the knee-hip biarticular units work as follows. After toe off, the swing phase begins as the human leg is protracted forwarded. The RF extends the knee joint during the swing phase in preparation for heel strike. The RF is a biarticular muscle and therefore affects the hip joint as well. As Figure 2-9 (c) shows, the RF also flexes the hip joint at the terminal stance phase and early swing phase. Therefore, the knee-hip anterior unit in the model works in a similar manner to the RF. Moreover, this biarticular unit transfers energy from the knee to hip joint. The HAM also works as a biarticular muscle as shown in Figure 2-9 (b). It generates force at the terminal swing phase and the early stance phase, and contributes to knee flexion around the time of heel strike. As can be seen in Figure 2-9 (c), the HAM acts as a hip extensor as well. This is the same function as the model's knee-hip posterior unit. Moreover, energy transfer from the knee to hip is allowed by this structure as well. Since I use a clutch in this unit, no energy dissipation occurs. Energy transferred from knee to hip joints for nine participants are shown in Table 2.2.1.

For the monoarticular hip muscle, the human leg comprises the iliopsoas (IL) and Gluteus maximus (GMAX), which act as a hip flexor and extensor, respectively. These muscles simply flex and extend the hip joint during walking, as do the model's hip flexor and extensor monoarticular units.

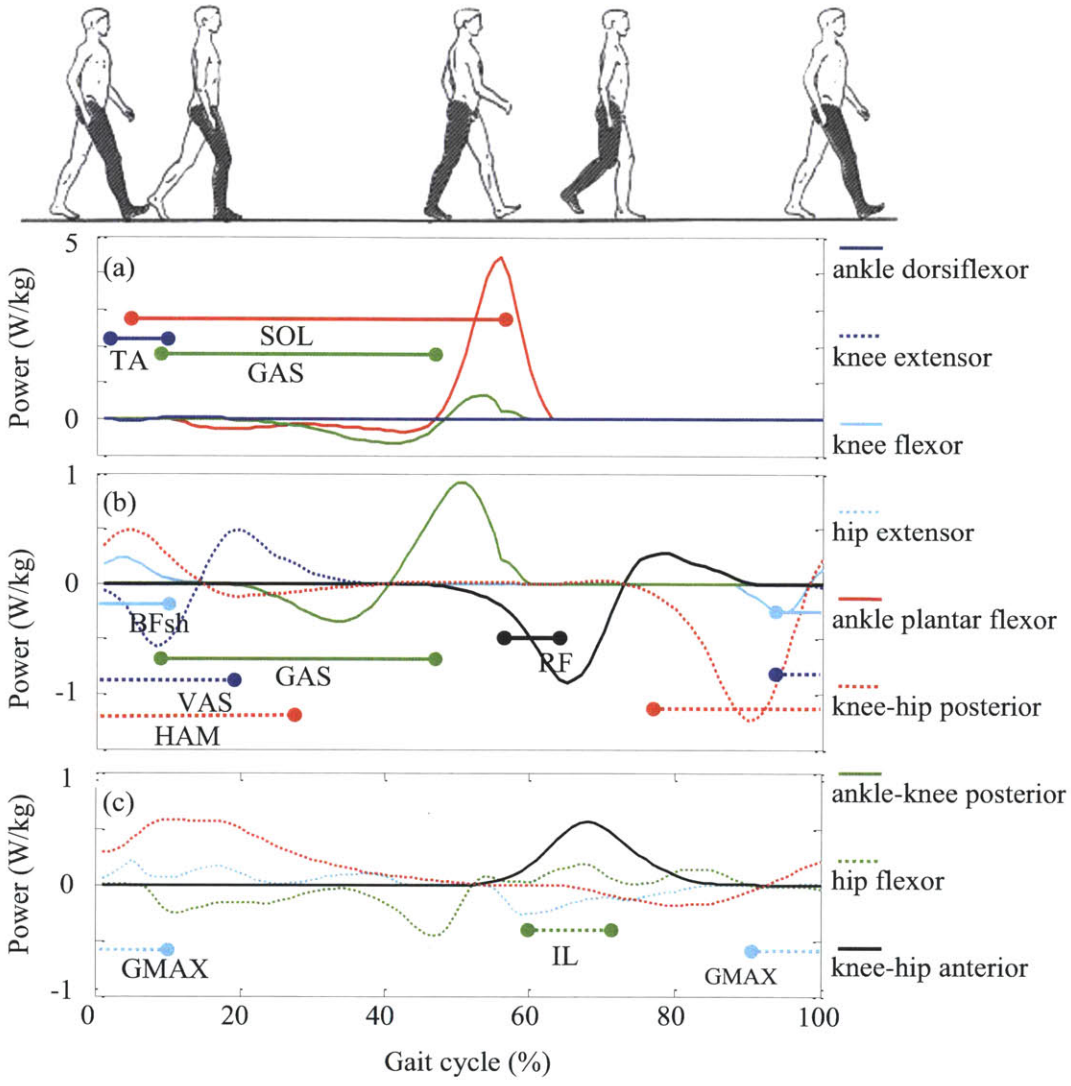

Figure 2-9: Spring contribution power curves and muscle EMG
Spring contribution power curves and muscle EMG for (a) ankle, (b) knee and (c) hip joints. All Power curves also indicate periods when clutches, actuators or variable damper are activated. Muscle EMGs are shown as horizontal solid lines with two circles at the edges. (Tibial anterior (TA), soleus (SOL), vastus mucles (VAS), gastocnemius (GAS), hamstrings (HAM), bicep femoris short head (BFsh), rectus femoris (RF), gluteus maximus (GMAX) and iliopsoas (IL)) EMG lines have the same color as the power curves that are anatomically and functionally equivalent.

Unit removed	R_k^2	c_{mt}	ET_{k-h}	ET_{k-a}	ActNet	ActPos	ActNeg	ElaPos
none (full leg model)	0.97	0.04	0.01	0.004	0.024	0.035	-0.01	0.051
hip ligament	0.97	0.06	0.008	0.004	0.029	0.046	-0.017	0.052
ankle dorsiflexor	0.97	0.05	0.008	0.004	0.027	0.038	-0.011	0.043
ankle-knee posterior	0.67	0.03	0.021	0.000	-0.014	0.0261	-0.028	0.055
knee extensor	0.50	0.06	0.004	0.005	0.033	0.046	-0.013	0.027
knee flexor	0.97	0.05	0.011	0.004	0.022	0.036	-0.015	0.052
knee-hip anterior	0.95	0.05	0.004	0.004	0.031	0.042	-0.011	0.039
knee-hip posterior	0.96	0.06	0.004	0.004	0.033	0.046	-0.013	0.034

Table 2.2: Effects of Component Removal
R_k^2, mechanical COT (c_{mt}), total energy transfer from knee to hip joint (ET_{k-h}), and from knee to ankle (ET_{a-k}), total net actuator work (ActNet), positive actuator work (ActPos), negative actuator work (ActNeg), positive spring work (ElaPos), of the model from which one unit is removed. Biological data of participant 1 is used for optimization.

According to Figure 2-9, at least one spring is always either storing or releasing elastic energy throughout the entire gait cycle per joint except for the ankle joint during the swing phase. Moreover, there are times when both agonist/antagonist pairs are engaged simultaneously. For example, from 18% to 38% gait cycle, both the mono knee extensor and the ankle-knee biarticular clutch are engaged at the same time. Actually, the energy stored at the mono knee extensor is transferred to the ankle-knee biarticular spring. Moreover, as mentioned earlier, some energy moves from the knee to the hip joint though biarticular activity. This energy transfer implies that the human leg makes use of the elasticity of MTUs.

2.3 Discussion

2.3.1 Alternative leg architecture

Humans have approximately 640 muscle-tendon units [52], while the model has many fewer elements. It is generally difficult to simply exploit dominant units to mimic human locomotion. the model can be justified by evaluating alternative leg architectures, for instance by removing one of the muscles and re-optimizing the parameters.

In each optimization, one of the clutches or actuators is erased and other components are kept in the model. Stiffness and the times for engaging clutches are re-optimized with the genetic algorithm and gradient search in the manner described in section two. As previous studies and the earlier work show, the ankle plantar flexor and hip extensor/flexor are necessary, six additional optimizations were conducted with the full leg model without ankle dorsiflexor, ankle-knee biarticular, knee extensor, knee flexor, knee-hip anterior, and knee-hip posterior.

Table 2.2 shows the knee torque R_k^2, mechanical COT (c_{mt}), total mechanical energy transfer from knee to hip (ET_{k-h}) and ankle to knee (ET_{k-a}), total net actuator work (ActNet), positive actuator work (ActPos), negative actuator work (ActNeg), positive spring work (ElaPos). The model without the hip ligament spring needs to generate more positive work at the hip actuators, which increases the mechanical work. The ankle dorsiflexor slightly affects the mechanical COT, as this causes the ankle actuators extra work. The R^2 of the knee torque dramatically decreases without the ankle-knee posterior or knee extensor. The effect of ankle dorsiflexor seems to be small. However, this unit is necessary, as this unit is the only muscle that generates negative torque during early stance phase. Regarding the knee flexor, it seems to affect R^2, ActNet, ActPos, ActNeg and ElaPos slightly, because the model has the knee-hip posterior as a knee flexor. However, this extra usage of the knee-hip posterior also causes extra activation of hip flexion and no hip extensor activation was observed. These engagements do not match with the muscle EMGs. Finally, as Figure 2-6 (b) and Table 2.2.1 show, knee-hip anterior and posterior transfer mechanical energy from knee to hip joint. Without these units, extra mechanical work from the hip extensor or flexor is needed. Therefore, the optimization also shows larger PosAct for the model without knee-hip anterior and posterior.

2.3.2 Is the leg model a plausible biological representation?

The model includes the ankle-knee posterior unit, which comprises springs, a series-clutch and an actuator. As mentioned above, the series-clutch and actuator generate force at the same time the gastrocnemius and soleus are activated in human normal

walking. Force from the clutch and actuator is also comparable to biological torque. As gastrocnemius and soleus lengths change uniquely during self-selected walking, so it is important to see how the biarticular unit behaves.

Ishikawa [26] reports the length change of the soleus and gastrocnemius with in-vivo measurement. In the simulation, the clutch is engaged from 10% to 55%. The soleus is lengthened from 12% to 47% and rapidly shortened after that. The in-vivo measurement also shows the same behavior.

2.3.3 Implications of leg model to robotic leg design

Motivated by the potential of advanced technology to improve QOL, researchers have developed computer-controlled, variable-damping prosthetic knees for transfermoral amputees such as the Blatchford Endolite Intelligent Prosthesis, the Otto Bock C-leg, and the Ossur Rheo. As the knee joint mainly generates negative work during the swing phase, the variable damper offers several advantages over mechanically passive designs, including enhanced knee stability and adaptation to different ambulatory speeds. However, the knee generates positive work during stance phase.

The model shows a good agreement with biological data instead of using a damper. During the swing phase, from 62% to 100% of gait cycle, knee-hip anterior and posterior springs store energy, or generate negative work. The stored energy is transferred to the hip joint through the biarticular units. The stored energy is also carried to the monoarticular knee extensor, which generates positive work during the stance phase. This agonist/antagonist and biarticular mechanism motivates the design of a prosthetic knee device with good economy and the capability of generating positive mechanical work as well as negative work for self-selected walking.

In addition to the knee dynamics, this model optimization indicates that each unit may be controlled by the body-environment interaction using local feedback such as a reflex mechanism rather than high-level neural system. In particular, each clutch can be engaged with a simple state machine whose state transitions with triggers of gait events. Figure 2-10 shows a state machine for SECs spanning at the knee joint. This is constructed based on the clutch engagement time shown in Figure 2-8 and 2-9.

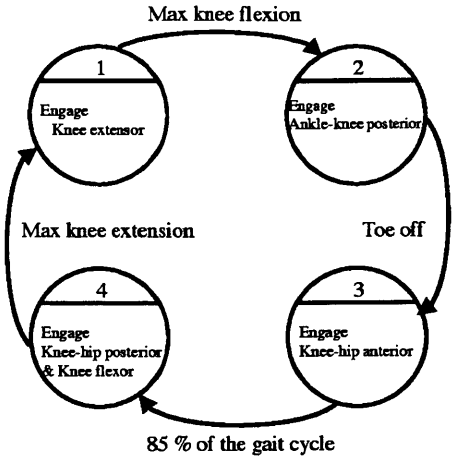

Figure 2-10: State machine for SEC spanning at the knee joint
The state machine engage the clutches, and each clutch is disengaged automatically when its series spring returns to its equilibrium point. The state transition is facilitated by gait event such as maximum knee flexion for the knee state transition from state 1 to 2. These transitions are all based on the clutches from the optimization (See Figure 2-8,2-9).

In the next chapter, further evaluation of the hypotheses is conducted with forward dynamics simulation, and this state machine controls the SECs spanning at the knee joint.

Chapter 3

Forward dynamic simulation

In the previous chapter, I focused on the importance of morphological aspects and required that all force sources function to provide perfect torque tracking across their respective joints, which results in almost perfect agreement with human biomechanics and walking economy for the self-selected speed walking, and reveals that the elasticity plays an important role to minimize metabolic COT. Moreover,the model also suggests that the SECs can be engaged by a simple state machine. To further evaluation of the hypotheses, in this chapter, a neuro reflex architecture of muscles for walking is investigated with forward dynamics simulation. The morphological parameters such as spring stiffness are also optimized together. To the end of this chapter, a neuro-musculoskeletal model is developed by replacing force sources with contractile elements of a Hill-type muscle and optimize control and model parameters simultaneously.

3.1 Method

3.1.1 Musculoskeletal leg model

The same two-dimensional musculoskeletal model proposed in the previous chapter is employed (see Figure 3-1) except for using Hill-type muscles [25, 62] instead of SEAs. The model was derived by inspection of the musculoskeletal architecture of

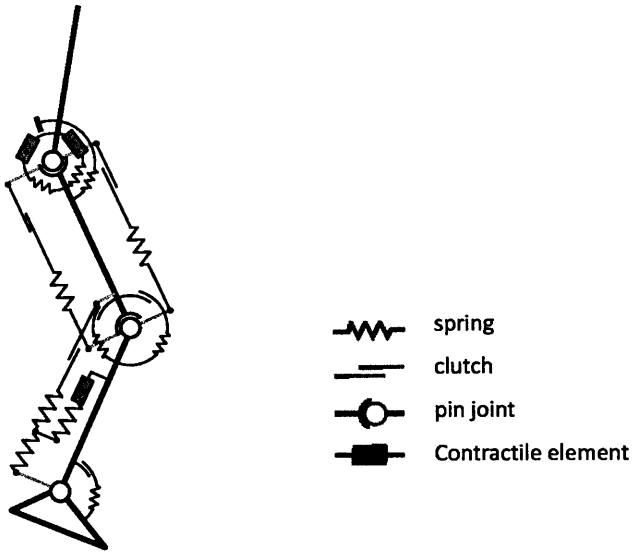

Figure 3-1: Musculoskeletal walking model
The same musculoskeletal as developed in the previous chapter (Figure 2-5) except for contractile elements of Hill-type muscle replaced with force sources. Only three muscles act about the model's ankle and hip joints. Series-elastic clutch units span the model's ankle, knee and hip in a musculoskeletal arrangement.

the human body, and SECs and Hill-type muscles are attached where main muscle groups are attached on a human body. The previous study revealed that, for self-selected walking speed, monoarticular hip and ankle muscles are required to capture the dominant mechanics at those joints, and only quasi-passive elements are necessary to capture the dominant features of knee joint mechanics. The mathematical muscle model is described in the next session. The seven segments of this under-actuated model (two feet, two shanks, two thighs and one head-arm-torso (HAT) segment) are simple rigid bodies whose mass parameters are estimated from nine human study participants shown in Table A.1 [23]. The clutches and muscles are all considered massless.

3.1.2 Muscle model

The hip extensor and flexor have linear springs in series with contractile elements. The ankle plantar flexor also has a series linear spring, but that spring also attaches to a second spring that spans the knee joint via a clutch mechanism (See Figure3-1). In forward dynamic simulation, an SEA unit (a force source with series spring) is replaced by a Hill-type muscle model, which is composed of series elasticity (SE) and contractile element (CE). Besides the SE and CE, the muscle model now includes parallel elasticity (PE), buffer elasticity (BE) components in a Hill-type MTU [62]. The force of the CE is a product of muscle activation α, CE force-length relationship $f_l(l_{CE})$, and CE force-velocity relationship $f_v(v_{CE})$, or

$$F_{CE} = \alpha F_{max} f_l(l_{CE}) f_v(v_{CE})) \tag{3.1}$$

$$f_l(l_{CE}) = \exp[c|\frac{l_{CE} - l_{opt}}{l_{opt} w}|^3] \tag{3.2}$$

$$f_v(v_{CE}) = \begin{cases} \dfrac{v_{max} - v_{CE}}{v_{max} + v_{CE}} & \text{if } v_{CE} \geq 0 \\ N + (N+1)\dfrac{v_{max} - v_{CE}}{7.56 K v_{CE} - v_{CE}} & \text{otherwise} \end{cases} \tag{3.3}$$

where F_{max} is the maximum isometric force, $l_{CE}(t)$ is the length of the CE, l_{opt} is the optimal length of the CE and $v_{CE}(t)$ is the CE velocity. In the force-length relationship $f_l(l_{CE})$, w describes the width of the bell-shaped curve and c is ln(0.05), fulfilling $f_l(l_{opt}(1 \pm w)) = 0.05$. The force-velocity relationship $f_v(v_{CE})$ follows the Hill equation [25] for muscle shortening ($v_{CE} < 0$), where $v_{max} < 0$ is the maximum contraction velocity and K is a curvature constant. Muscle lengthening ($v_{CE} \geq 0$) is characterized by an equation based on Aubert [17], where N is the dimensionless amount of force F_{CE}/F_{max} reached at a lengthening velocity $v_{CE} = -v_{max}$. These values are shown in Table 3.1.

Based on this product approach, we compute the muscle fascicle dynamics by integrating the CE velocity. The muscle activation α relates to a neutral input $S(t)$

Parameter	Description	Value
w	width of the bell shaped f-l curve	0.56
c	shape of bell shaped curve near the extremes of the bell	0.05
N	muscle force (in units of F_{max}) at maximum lengthening velocity $v_{CE} = v_{max}$	1.8
K	curvature constant	5

Table 3.1: Parameters for Hill-type muscle model
These parameters define the shape of the force-length and force-velocity function. The values are employed from [17].

with a first order differential equation describing the excitation-contraction coupling

$$\tau \frac{d\alpha(t)}{dt} = S(t) + prestim - \alpha(t) \tag{3.4}$$

where τ is a time constant, and *prestim* is a predefined pre-stimulation. The maximum isometric force and optimal length of ankle plantar flexor muscle, F_{max}^{ap} and l_{opt}^{ap} are variables for the optimization while the remaining values are chosen from the literature [13, 21].

3.1.3 Clutch and muscle controllers

The muscles and clutches are controlled by simple feedback controllers and state machines. Force, length and velocity feedback loops are constructed for the ankle plantar flexor muscle and two kinds of position controllers are used for two hip muscles. The state transitions are facilitated by the human model and its interaction with the walking surface, and each clutch is engaged or muscle activated according to the state. The state machines were constructed such that clutch engagements were triggered by gait events suggested by our previous optimization results (Figure 2-8). In the next section, two reflex controllers for three muscles and three state machines for three joints are constructed.

3.1.4 Force, length and velocity feedback controller for the ankle plantar flexor

During the stance phase, especially at the terminal stance phase, the soleus muscle generates a large amount of positive power to push off the ground [6, 18]. Empirical measurement demonstrated importance of force and length-related reflex responses [18, 3, 10]. In order to replicate this behavior, force, length and velocity feedback from the muscle fascicle is adopted for ankle plantar flexor control. Figure 3-2 shows a reflex architecture of the ankle joint during the stance phase. In this figure, force, velocity and length are all normalized by maximum isometric force, maximum velocity and optimal length, respectively. Under force, length and velocity feedback, the stimulation of the ankle plantar flexor $S^a(t)$ is calculated as follows

$$\begin{aligned} S^{ap}(t) = S_0^{ap} + G_F^{ap} F^{ap}(t - \Delta t^{ap}) u(F^{ap} - F_0^{ap})) + \\ G_l^{ap} l^{ap}(t - \Delta t^{ap})) u(l^{ap} - l_0^{ap}) + \\ G_v^{ap} v^{ap}(t - \Delta t^{ap})) u(-v^{ap}) \end{aligned} \tag{3.5}$$

where S_0^{ap} is a constant pre-stimulation, $G_F^{ap}, G_v^{ap}, G_l^{ap}$ are force, velocity and length feedback gains, F^{ap} and F_0^{ap} are the measured muscle force and force threshold, l^{ap} and l_0^{ap} are the measured CE length and length threshold, v^{ap} is the measured CE velocity and Δt is a time-delay for the feedback loop. The function $u()$ is a unit step functions that ensure the feedback terms are only enabled when the argument of this function is positive. This feedback control is turned on only after foot flat (FF) during the stance phase and is turned off at the time of toe off (TO). During swing phase, the ankle joint is controlled with a simple proportional-derivative (PD) control with low gain to keep the ankle angle equal to $\hat{\theta}^a$ in preparation for heel strike (HS). The ankle state machine is shown in the following section. In the force and velocity feedback control, $G_F^{ap}, G_l^{ap}, G_v^{ap}, \Delta t^{ap}, F_0^{ap}, l_0^{ap}$ and $\hat{\theta}^a$, are optimized while the remaining parameters are taken from the literature [21].

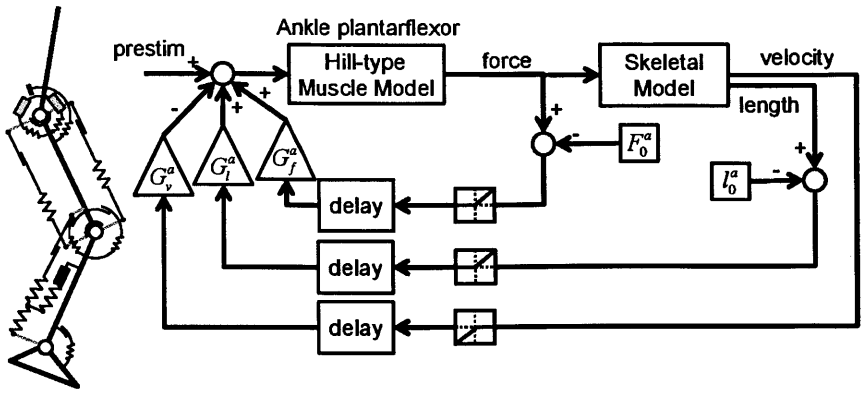

Figure 3-2: Ankle reflex architecture
The input stimulation for the ankle plantar flexor is composed of three feedback loops, force, length and velocity of the contractile element. The force, length and velocity described in this figure are normalized by the maximum isometric force, the optimal length, and maximum contraction velocity, respectively. The mathematical expression is shown in Eq. 3.5.

3.1.5 HAT and thigh segment PD Feedback controller for the hip muscles

Balancing the HAT segment is generally considered as a multisensor integration task from the vestibular organs, visual cues, and proprioception from the leg muscles [38]. While this complex integration seems critical to control standing, it may not be required during locomotion [44]. On the other hand, Gunther [39], Geyer and Herr [21] stabilized the HAT segment of a human walking model only by activating the hip muscles proportional to the velocity of the HAT segment and to its forward lean in the inertial system. As my position is to develop a simple walking model, I construct hip controllers based on these two studies.

I construct two different controllers of hip muscles for the stance and swing phase as shown in Figure 3-3. Since the hip flexor and extensor are attached to the HAT segment directly, these two muscles are used to balance the HAT segment mainly during stance phase. The hip flexor and extensor are stimulated with a PD signal of the difference between HAT's pitch angle θ_{HAT} with respect to gravity and the

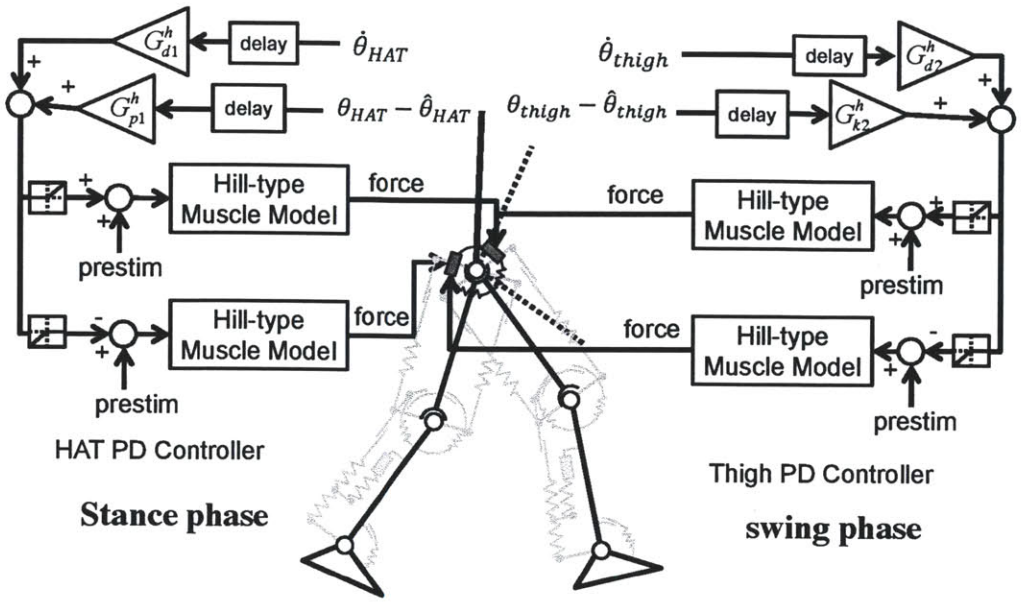

Figure 3-3: Hip reflex architecture
There are two types of feedback controller for an agonics/antagonics pair of hip muscles, HAT PD controller for the stance phase and thigh PD controller for the swing phase. They have exactly same reflex structures but different reference angles and different feedback gains. The reference angles are shown as $\hat{\theta}_{HAT}$ and $\hat{\theta}_{thigh}$ for HAT PD and thigh PD controller respectively.

reference angle $\hat{\theta}^{HAT}$ as follows

$$S^h_{stance}(t) = -G^h_{p1}\{\hat{\theta}^{HAT} - \theta^{HAT}(t-\Delta t^h)\} - G^h_{d1}\dot{\theta}^{HAT}(t-\Delta t^h)) \quad (3.6)$$

$$S^h_{extensor}(t) = \begin{cases} S^h_{stance}(t) & if \quad S^h_{stance} > 0 \\ 0 & otherwise \end{cases} \quad (3.7)$$

$$S^h_{flexor}(t) = \begin{cases} -S^h_{stance}(t) & if \quad S^h_{stance} < 0 \\ 0 & otherwise \end{cases} \quad (3.8)$$

where G^h_{p1} and G^h_{d1} are the proportional and derivative gains, and Δt^h is a time-delay of the feedback loop.

During the swing phase, the swing leg needs to be carried forward in preparation

for HS. The hip joint is controlled so that the thigh pitch angle θ^{thigh} reaches a reference angle $\hat{\theta}^{thigh}$ as follows:

$$S^h_{swing}(t) = -G^h_{p2}\{\hat{\theta}^{thigh} - \theta^{thigh}(t - \Delta t^h)\} - G^h_{d2}\dot{\theta}^{thigh}(t - \Delta t^h)) \quad (3.9)$$

$$S^h_{extensor}(t) = \begin{cases} S^h_{swing}(t) & if \quad S^h_{swing} > 0 \\ 0 & otherwise \end{cases} \quad (3.10)$$

$$S^h_{flexor}(t) = \begin{cases} -S^h_{swing}(t) & if \quad S^h_{swing} < 0 \\ 0 & otherwise \end{cases} \quad (3.11)$$

where G^h_{p1} and G^h_{d2} are the proportional and derivative gains, $\hat{\theta}^{thigh}$ is a reference thigh angle in the global axis, and Δt^{thigh} is a time-delay. In the swing phase, the hip flexor is mainly activated to bring the swing leg forward. Moreover, after the maximum knee extension, humans generates traction torque in preparation for the HS. In order to replicate this, I use two different reference angles $\hat{\theta}^{thigh}_1$ and $\hat{\theta}^{thigh}_2$ for before and after the maximum knee extension, respectively, where $\hat{\theta}^{thigh}_1 \leq \hat{\theta}^{thigh}_2$. In the hip position controller, $G^h_{p1}, G^h_{d1}, \hat{\theta}^{HAT}, G^h_{p2}, G^h_{d2}, \hat{\theta}^{thigh}_1$ and $\hat{\theta}^{thigh}_2$ are optimized while the remaining parameters are taken from the literature [21]. These HAT and thigh PD controllers are switched by the hip state machine.

3.1.6 State machine

Figure 3-4 shows state machines for controlling (a) the ankle, (b) knee and (c) hip joints. The knee state machine is same as Figure 2-10 except for the transition from the state 3 to 4 triggered by the knee angle. This is because of the difficulty of detecting the 85% of gait cycle during walking. The state machines turn on/off or switch the muscle feedback controllers, and engage the clutches. Each clutch is disengaged automatically when its series spring returns to its equilibrium point.

The ankle state machine is composed of three states. In State 1, which begins at HS, the clutch in the ankle dorsiflexor is engaged. The controller transitions from State 1 to State 2 at FF, at which time the feedback control is initiated. These

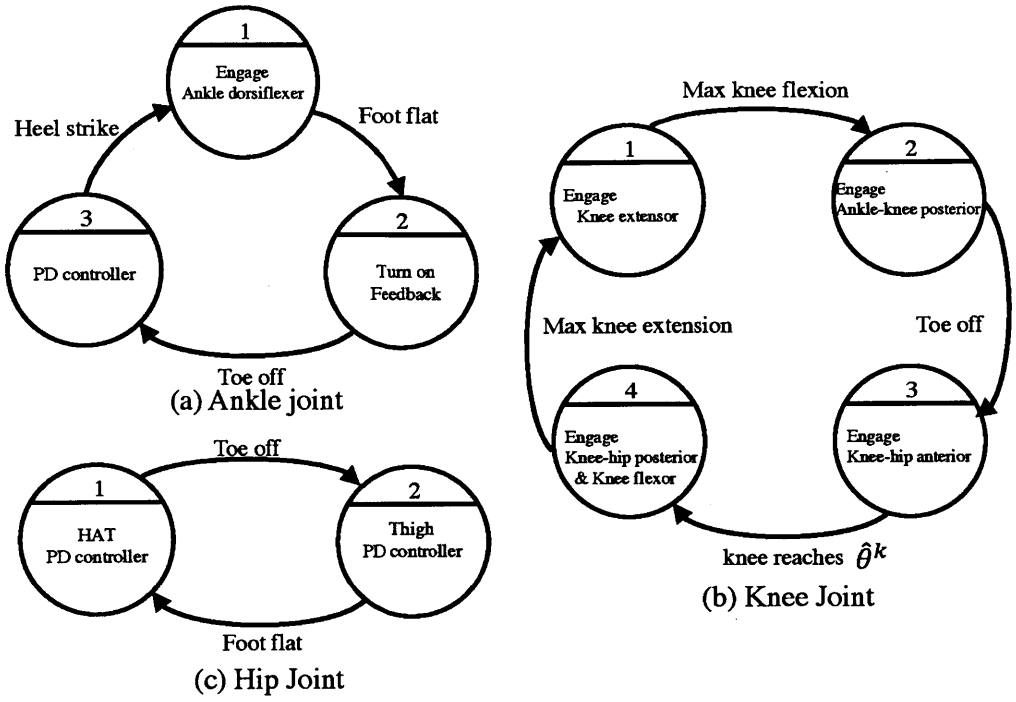

Figure 3-4: State machine
The state machines for (a) the ankle, (b) knee and (c) hip joints. The state machines turn on/off the muscle feedback controllers and engage the clutches. Each clutch is disengaged automatically when its series spring returns to its equilibrium point. The state transition is facilitated by gait event such as HS for the ankle state transition from state 3 to 1, and maximum knee flexion for the knee state transition from state 1 to 2. These transitions are all based on the clutches and force sources actuation from the previous optimization (See Figure 2-8,2-9).

transitions are established also based on the results of the previous optimization (Figure 2-8 and 2-9). The controller transitions from State 2 to State 3 at toe off (TO). In State 3, the feedback controller is turned off and the low-gain PD controller is applied at the ankle joint to keep the ankle angle equal to $\hat{\theta}^a$ in preparation for HS. At the next HS, the controller transitions from State 3 back to State 1.

The knee state machine controller consists of four states. The controller transitions from State 1 to State 2 at maximum knee flexion during the stance phase following HS. In State 2, the ankle-knee posterior clutch is engaged. The transition from State 2 to State 3 is triggered by TO after which the knee-hip anterior is engaged. The

controller transitions from State 3 to State 4 when the knee angle reaches $\hat{\theta}^k$ after maximum flexion during the swing phase. The knee-hip posterior and knee flexor are engaged in State 4. Finally, the controller goes back to State 1 from State 4 when the knee joint reaches maximum extension in swing phase. The knee extensor is engaged in State 1.

The hip state machine controller includes only two states. The hip controller transitions from State 2 to State 1, at the time of the FF, and from State 1 to State 2 at the TO. The hip muscles are controlled with the HAT and thigh segment PD controllers in States 1 and 2, respectively.

3.1.7 Optimization strategy

The model has a total of 27 variables: 10 spring constants, the hip ligament engagement angle, 12 Hill-type muscle control parameters, and four reference angles for the state machine. Parameters are evaluated with a walking forward dynamics simulation. In order to consider both joint biomechanics and metabolic COT, I adopt an elitest non-deterministic sorting genetic algorithm (termed NSGA-II) [31, 11, 12], and the following objective function is used as well as Eq.3.12:

The cost function is defined as follows:

$$cost_1 = \begin{cases} \dfrac{10}{D+N} & \text{if } t_s \geq 20 \\ c_{et} & \text{otherwise} \end{cases} \tag{3.12}$$

where t_s is the last time of walking simulation, and D is the normalized walking distance, N is the number of steps, and c_{et} is metabolic COT. Each individual is evaluated after a forward dynamics simulation. When the simulation time reaches 20 seconds, I assume the model walks in steady state and the simulation is terminated, and then next individual is simulated. When the model falls down in less than 20 seconds, the simulation is terminated immediately and the next simulation starts. Metabolic COT is defined as

$$c_{et} = \frac{\sum_i \int p(v^i/v^i_{max}) F^i_{max} \alpha^i(t) dt}{MgD} \tag{3.13}$$

where $p(v_{ce}/v_{max})$ is the normalized metabolic power function in terms of normalized muscle fascicle velocity, α^i is ith muscle activation, and F^i_{max} and v^i_{max} are maximum force and maximum velocity of the ith muscle, respectively. This metabolic cost function is employed from Pkrishnaswamy's work [45]. The optimizer uses the first objective function in Eq. 3.12 to find parameters that enables the model to walk for more than 20 seconds without falling down. If the musculoskeletal model is capable of walking for more than 20 seconds, the second objective function in Eq. 3.12 is used. The value of the first cost in Eq.3.12 is always less than that of the second cost, so the optimizer selected parameters that enables both robust and economical walking [22, 40]. As the second objective function is the following:

$$cost_2 = 1 - \frac{\sum_{i=a,k,h} R^i_{angle}}{3} \tag{3.14}$$

where R^i_{angle} is a cross-correlation coefficient of ith joint angle between the model and biological data. Moreover, as the self-selected walking speed of all participants in Table A.1 is between 1.2 to 1.35m/s, only individuals within this range are preserved in the next generation. This is a similar method of e-constraint of optimization [20, 12] and this shortens the amount of computation as well as makes the optimization easier to be converged. I use the same body mass, height, length, weight, moment of inertia of each segment of participant shown in Table A.1.

3.2 Results

3.2.1 Determination of the optimal solution

Figure 3-5 shows the results of the NSGA-II optimization with two objective cost: metabolic COT and R of three joint angles of one representative participant (participant 1 in Table A.1). The blue dots denote all individual solutions which can walk for more than 20s in the forward dynamic simulation, and the square and circle

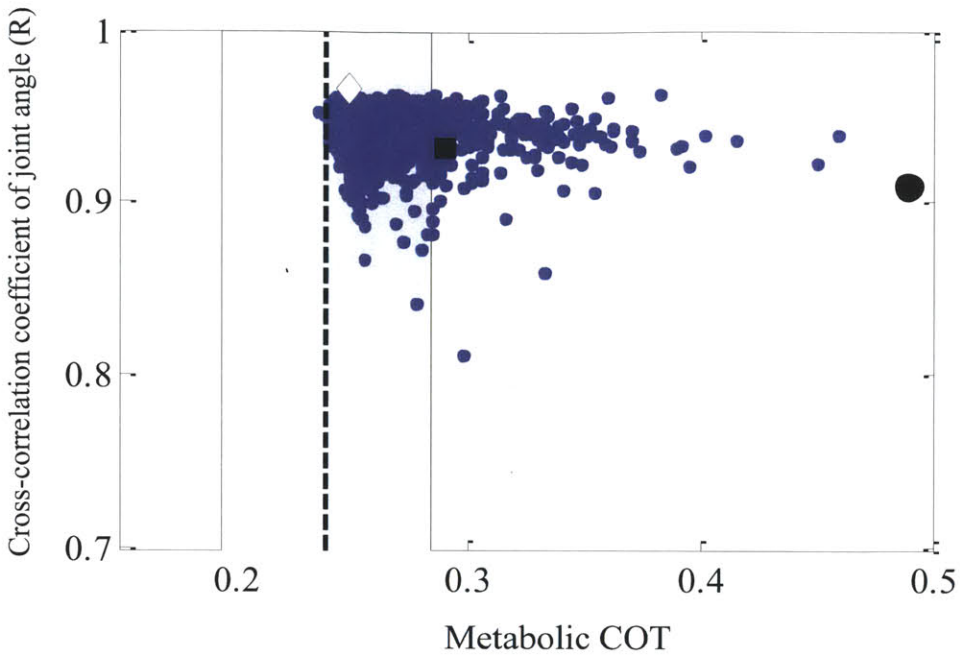

Figure 3-5: Relationship between metabolic COT vs R (Participant 1)
Each blue dots are individuals which can walk at least for 20 seconds in the forward dynamics simulation of the one representative participant (Participant 1 in Table A.1). The dashed line and shaded area is the average of human metabolic COT and the range within one standard deviation from the average [24]. The square and circle are the models from [21] and [5], respectively.

denote the models from literature (square: Geyer and Herr model [21], circle: Anderson and Pandy model [5], respectively. These two studies are known for excellent representations of human walking models. Obviously, the optimization found better solutions in terms both of metabolic COT and R. The dashed line and shaded area is the average of human metabolic COT and the range within one standard deviation from the average [24]. My goal is to find a simple musculoskeletal model which can walk with as low metabolic COT as that of humans, as well as good agreement with human biomechanics. Therefore, I here define the individual with the best R value in this range as the optimal solution (a diamond in Figure 3-5.) The relationship between metabolic COT and R of the other eight participants (participants $2 \sim 9$ in Table A.1) are shown in Figure 3-6. The dashed line and shaded area indicates the average of human metabolic COT and area within one standard deviation from the

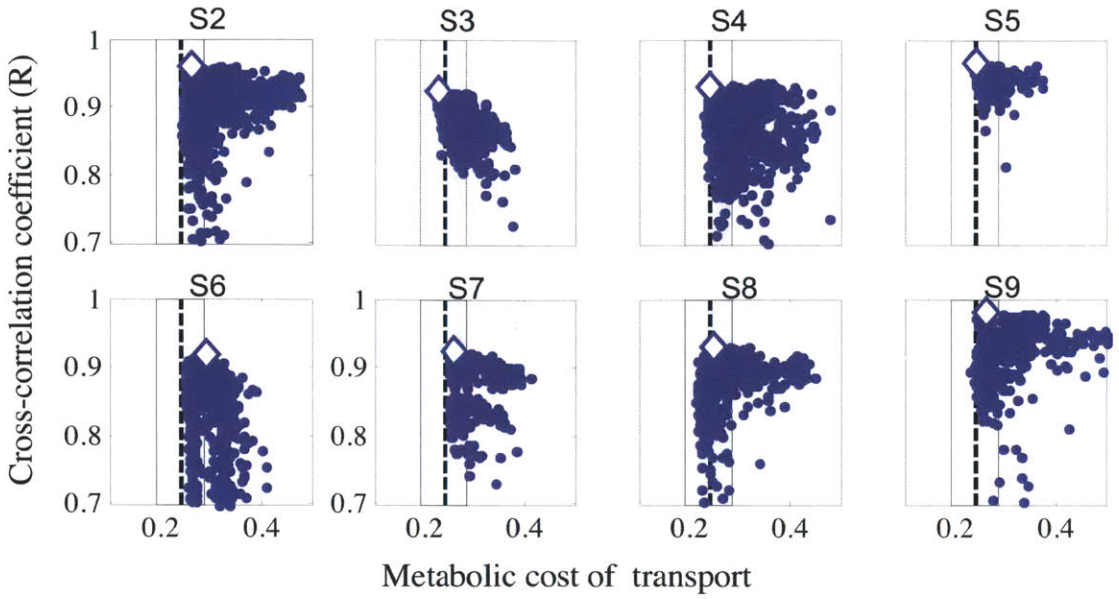

Figure 3-6: Relationship between metabolic COT vs R (Participant $2 \sim 9$)
Each blue dots are individuals which can walk at least for 20 seconds in the forward dynamics simulation of eight participant (Participant $2 \sim 9$ in Table A.1). The dashed line and shaded area is the average of human metabolic COT and the range within one standard deviation from the average [24].

average, respectively. The diamond is the optimal solution chosen with the same criteria as mentioned above. Even though they have different mass, height, and segment properties, these plots indicate all participants shows good agreement with biological angle as well as metabolic COT comparable with that humans.

	Musculoskeletal Model	Human
Walking speed (m/s)	1.28 ± 0.04	1.27 ± 0.11
Step length (m)	0.80 ± 0.07	0.67 ± 0.06
Stride time (s)	1.25 ± 0.04	1.04 ± 0.10

Table 3.2: Walking speed, step length and stride time of the model and human
Simulation data are the average and standard deviation of musculoskeletal model of nine participants in Table A.1. Human data are measured from the same participants.

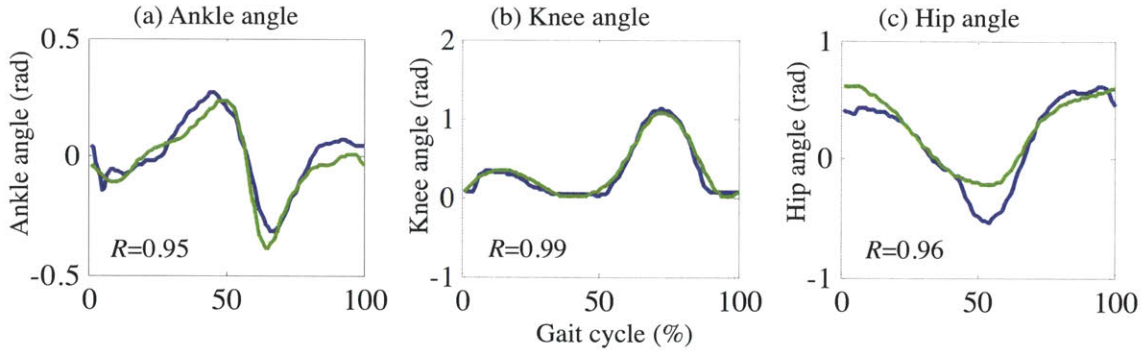

Figure 3-7: Joint angle agreement
(a) ankle angle, (b)knee angle, and (c)hip angle. The blue and green curves are the average of 10 steps in the steady state walking in the simulation and human biological data of one representative participant (Participant 1 in Table A.1). The dotted curves are one standard deviation from the average. The R values of the simulation and biological data are 0.95 for ankle angle, 0.99 for knee angle, 0.96 for hip angle,

3.2.2 Kinematics

Walking speed, step length, and stride time

The optimal model's average walking speed, stride time, step length, of nine participants are shown in Table 3.2 along with values from a weight and height-matched walking human. The current computational set-up results in the close walking speed with wider step length and longer stride time than human self-selected walking data.

Joint angle agreement

In Figure 3-7, (a) the ankle angle, (b) the knee angle, and (c) the hip angle are plotted versus percent gait cycle of one representative participant (Participant 1 in Table A.1). Each curve begins at HS and ends with the next HS of the same leg. In the figure, blue and green curves are simulation results and biological data from a weight and height-matched walking person, respectively (human data obtained from the literature [23]). Dotted curves are one standard deviation from the mean. These data are the averages of 10 steps in steady state walking. To quantify the agreement, I use the cross-correlation coefficients of model and human trajectories. $R = 1$ shows a perfect

participant	R^a_{angle}	R^k_{angle}	R^h_{angle}
1	0.95	0.99	0.96
2	0.86	0.97	0.95
3	0.87	0.95	0.97
4	0.76	0.94	0.97
5	0.78	0.97	0.97
6	0.95	0.97	0.96
7	0.78	0.92	0.95
8	0.79	0.92	0.94
9	0.90	0.92	0.94
average	0.85	0.95	0.96
s.d.	0.07	0.02	0.01

Table 3.3: Cross-correlation coefficient of angle between simulation and biological data
These R values are calculated using the biological data and simulation result of nine participants shown in Table A.1. R^a_{angle}, R^k_{angle}, R^h_{angle} are the cross-correlation coefficients of the ankle, knee, and hip angle, respectively.

agreement, whereas $R = 0$ indicates no agreement. The model makes quantitative predictions about ankle, knee, and hip mechanics, since the joint kinetics shows a good agreement on all joints ($R = 0.95$ for ankle angle, $R = 0.99$ for knee angle, $R = 0.96$ for hip angle). The other participants' R values are shown in Table 3.3 which shows a good agreement on all joint angle as well.

State transition

The model's state machines performed properly throughout the walking cycle. Figure 3-4 shows joint state transition of one representative participant (participant 1 in Table A.1) for two walking cycles during steady state walking (from 9.5 to 12.5 seconds in the forward dynamics simulations). The walking leg motion of one gait cycle is also shown beyond the plots. The controller transitions from state to state facilitated by gait events: (1)HS, (2)FF, (3)maximum knee flexion in the stance phase, (4)the other leg's HS, (5)TO, (6)knee angle reaches the knee reference angle $\hat{\theta}^k$ after maximum flexion during the swing phase, (7)knee maximum extension, The control system sequenced though this pattern during each walking cycle.

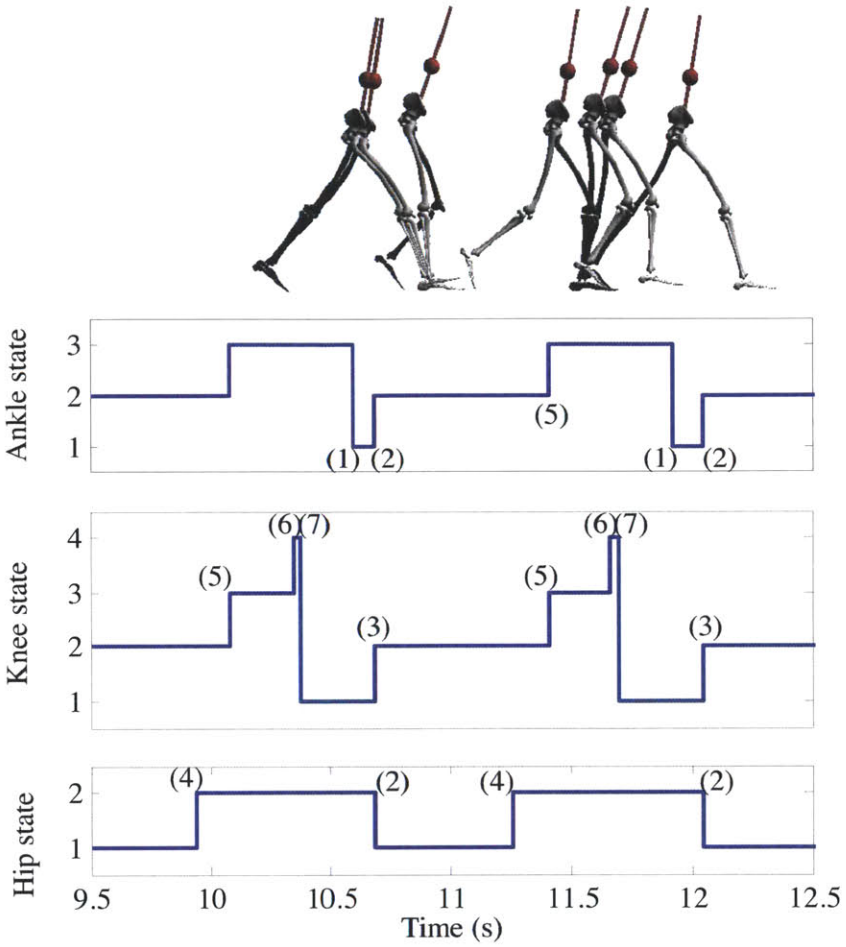

Figure 3-8: State transition

This state transition is cropped from the simulation result of the one representative participant (Participant1 in Table A.1). The controller transitions from state to state facilitated by gait events: (1)HS, (2)FF, (3)maximum knee flexion in the stance phase, (4)the other leg's HS, (5)TO, (6)knee angle reaches the knee reference angle $\hat{\theta}^k$ after maximum flexion during the swing phase, (7)knee maximum extension, The control system sequenced though this pattern during each walking cycle.

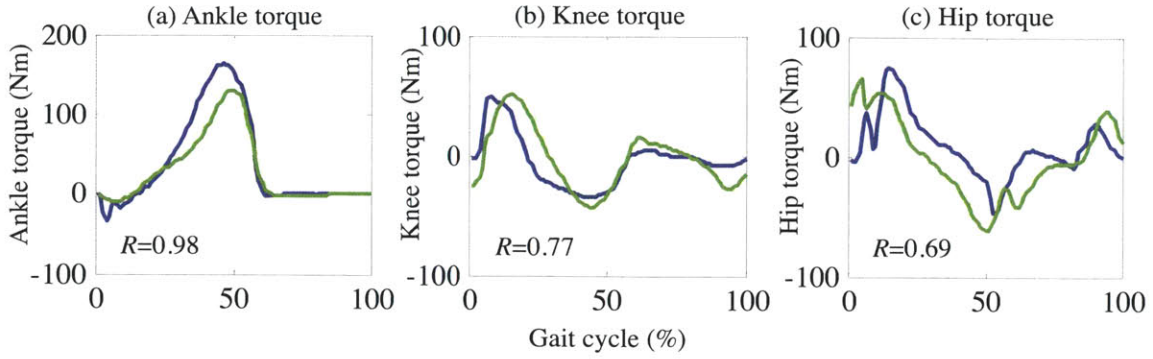

Figure 3-9: Joint torque agreement
(a)ankle torque, (b)knee torque and (c)hip torque. The blue and green curves are the average of 10 steps in the steady state walking in the simulation and human biological data of one representative participant (Participant 1 in Table A.1). The dotted curves are one standard deviation from the average. The R values of the simulation and biological data are 0.98 for ankle torque, 0.77 for knee torque, and 0.69 for hip torque.

3.2.3 Kinetics

Joint torque agreement

In Figure 3-9, (a) the ankle torque, (b) the knee torque, and (c) the hip torque angle are plotted versus percent gait cycle of one representative participant (Participant 1 in Table A.1). Each curve begins at HS and ends with the next HS of the same leg. In the figure, blue and green curves are simulation results and biological data from a weight and height-matched walking person, respectively (human data obtained from the literature [23]). Dotted curves are one standard deviation from the mean. These data are the averages of 10 steps in steady state walking. The cross-correlation coefficient R is again used to quantify the agreement. R values of the ankle torque shows good agreement ($R = 0.98$ for the ankle joint). However, R values of knee and hip joint torque do not show significant agreement, relatively($R = 0.77$ for the knee joint, and $R = 0.69$ for the hip joint). These trends can also be seen in other participants' R values shown in Table 3.3. R values of the ankle torque shows good agreement ($R = 0.84$), while R values of knee and hip joint torque does not show significant agreement ($R = 0.59$ for knee torque, $R = 0.46$ for hip torque). This may

participant	R^a_{torque}	R^k_{torque}	R^h_{torque}
1	0.98	0.77	0.69
2	0.78	0.51	0.14
3	0.91	0.61	0.47
4	0.67	0.23	0.27
5	0.72	0.52	0.47
6	0.96	0.83	0.65
7	0.81	0.48	0.45
8	0.83	0.53	0.34
9	0.96	0.81	0.62
average	0.84	0.59	0.46
s.d.	0.11	0.19	0.10

Table 3.4: Cross-correlation coefficient of torque between simulation and biological data
These R values are calculated using the biological data and simulation result of nine participant shown in Table A.1. R^a_{torque}, R^k_{torque} ,R^h_{torque} are the cross-correlation coefficients of the ankle, knee, and hip torque, respectively.

be caused by noise and error of sensory information of the motion capture system and inversed dynamics calculation. In fact, when a joint angle is geometrically far from the ground surface, inversed dynamics calculation results in larger error in torque. The previous studies also show a poor agreement on hip and knee joint torque [5, 21].

Ground reaction force

Figure 3-10 shows vertical and horizontal GRF of biological and simulation of the one representative participant (participant1 in Table A.1). Light and deep blue curves are vertical GRF of simulation and biological data, respectively, and light and deep green curves are horizontal GRF of simulation and biological data, respectively. The dotted curves are one standard deviation from the average curve. These data are normalized by body weight. Simulated GRFs are average of 10 steps in steady state. The TO occurs at 62% of the gait cycle, which is the exactly same as that of the biological data. The curve starts with the heel strike and end with the next heel strike of the same leg. Here, the vertical GRF in stance shows the M-shape pattern characteristic for walking gaits, indicating similar CM dynamics of model and humans for steady-state walking except for the small peak of the simulation vertical GRF at the 5%.

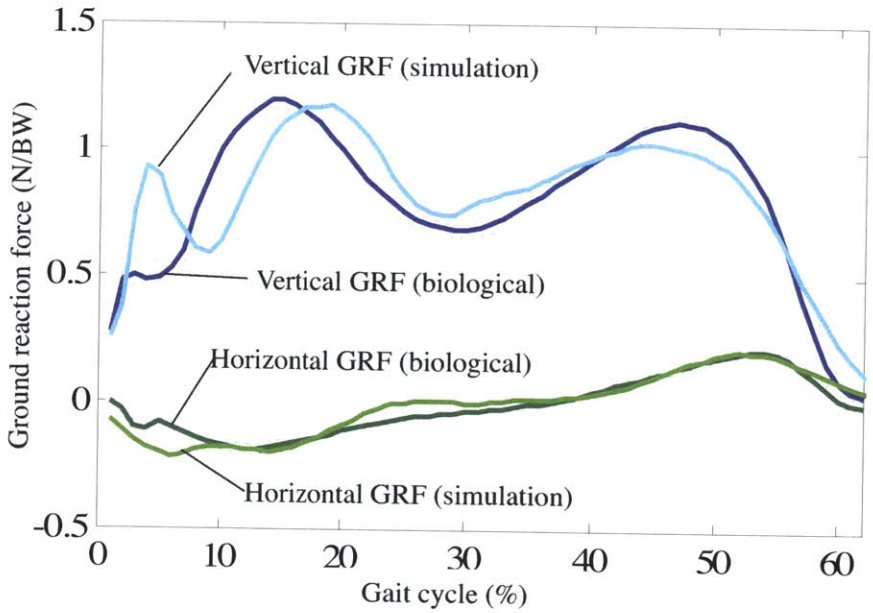

Figure 3-10: Ground reaction force
Vertical and horizontal GRF of biological and simulation of one representative participant (participant1 in Table A.1). The data during the stance phase (0 $\sim$ 62% of gait cycle) are shown in this plot. Light and deep blue curves are vertical GRF of simulation and biological data, respectively, and light and deep green curves are horizontal GRF of simulation and biological data, respectively. The dotted curves are one standard deviation from the original curve. These data are normalized by body weight. Simulated GRFs are average of 10 steps in steady state.

This indicates the model has earlier knee maximum flexion in the stance phase than human. This can also be seen in the Figure 3-7 (b). The knee torque shown in Figure 3-9 (b) also show the peak knee extension at 5 % of the gait cycle. This may happen because energy exchange among kinetic, potential and elastic domain does not occur correctly, and some amount of energy is absorbed by the ground. On the other hand, the horizontal GRF greatly agrees with that of the human.

	metabolic COT	mechanical COT
1	0.28	0.039
2	0.20	0.023
3	0.24	0.032
4	0.19	0.024
5	0.20	0.025
6	0.24	0.035
7	0.24	0.036
8	0.25	0.038
9	0.24	0.036
average	0.22	0.031
s.d.	0.02	0.006

Table 3.5: Metabolic and mechanical cost of transport
The metabolic and mechanical COT are calculated from the simulation result of nine participant shown in Table A.1.

3.2.4 Energetics

Metabolic and mechanical COT

Table 3.5 shows the metabolic and mechanical COT of walking as predicted by the leg model. The mean values of nine participants are 0.22 and 0.031, respectively. On the other hand, the metabolic and mechanical COT human walking has been estimated at 0.2 and 0.05, respectively [Donelan et al. 2002]. However, this mechanical COT was calculated by integrating the product of the CM velocity and ground reaction force, which includes contribution of internal work and elasticity as well as actual muscle mechanical work. This is discussed more in the next section.

Energy transfer

In the previous chapter, I showed that, as a biarticular unit spans multiple joints, mechanical energy can be carried from one joint to another: energy stored in the spring at one joint can be reused at the different joint (Table 2.2.1). Table 3.6 shows normalized energy transfer from knee to hip (ET_{k-h}), and ankle to knee (ET_{a-k}) of all participantes, which are normalized by body weight and leg length. All participant shows small amount of energy transferred from the ankle to knee joint, ET_{a-k}.

	ET_{k-h}	ET_{a-k}	$REC(\%)$	ActNet	ActPos	ActNeg	ElaPos
1	0.002	0.000	43.7	0.026	0.034	-0.008	0.048
2	0.002	0.002	65.6	0.009	0.017	-0.008	0.038
3	0.003	0.005	55.8	0.018	0.025	-0.007	0.038
4	0.001	0.000	41.0	0.010	0.018	-0.008	0.029
5	0.001	0.000	59.2	0.010	0.020	-0.010	0.032
6	0.004	0.001	78.8	0.022	0.028	-0.007	0.049
7	0.003	0.002	61.7	0.026	0.033	-0.008	0.048
8	0.004	0.002	69.6	0.027	0.034	-0.007	0.048
9	0.003	0.002	61.7	0.026	0.033	-0.008	0.048
average	0.003	0.002	59.7	0.018	0.026	-0.008	0.041
s.d.	0.001	0.001	11.9	0.007	0.007	0.001	0.008

Table 3.6: Walking model evaluation
Total energy transfer from knee to hip (ET_{k-h}) and from knee to ankle (ET_{a-k}), percentage recovery (%REC), net actuator work (ActNet), positive actuator work (ActPos), negative actuator work (ActNeg), positive spring work (ElaPos). Values listed for 9 study participants (Table A.1). All energy quantities are normalized by the product of leg length and body weight, except for the mechanical COT which is normalized by the product of stride length and body weight.

Specifically, participant 1 transfers 0.13J of mechanical energy from the ankle to knee joint, while the previous optimization shows 2.5 J for the same value. The amount of energy transfer from the knee to hip joint ET_{k-h} is relatively small as well. The actual breakdown of the energy transfer of participant 1 is 1.8J and 0.1J of mechanical energy transferred through the knee-hip anterior and posterior, respoectively, while the previous optimization shows 3.4J and 4.3J, respectively for the same values. The other pariticipants also use the knee-hip posterior little to transfer the mechanical energy.

Whole-body mechanical energetics

Figure 3-11 shows the average of the participant 1 potential and kinetic energy variations in time during one gait cycle from the heel strike to the another heel strike of the same leg, as well as variations in elastic energy storage from both legs as estimated by the model. These are dimensionless values normalized by body weight and CM height. The red and green curves are total energy stored by all elastic elements

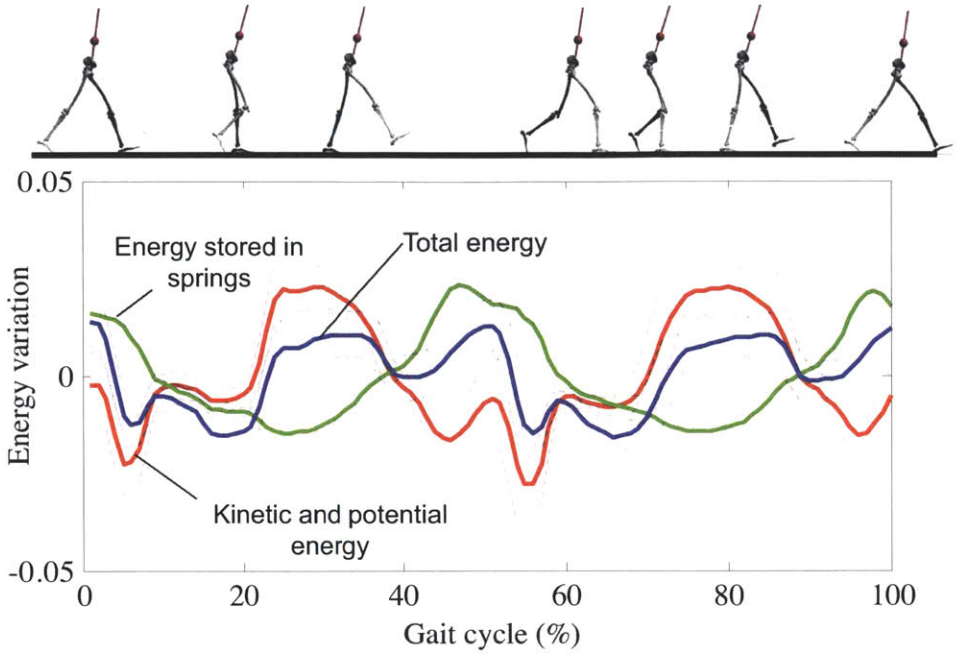

Figure 3-11: Potential, kinetic and elastic energy variation
Energy is dimensionless normalized by body mass and center of mass height of one representative participant (Participant 1 in Table A.1). The red curve denotes energy which includes potential and kinetic energy at the center of mass as well as kinetic energy at the segments relative to the center of mass. The green curve is elastic potential energy stored in springs. The blue curve is total energy in the model. Each dotted line is one standard deviation from the solid line.

in the model and the sum of potential and kinetic energy of the body, respectively, and the blue curve is the sum of these two energy curves. Elastic energy storage is maximized around 95% and 45% of the gait cycle, while kinetic and potential energy is maximuzed at 28% and 78 % of the gait cycle. Their peaks are shifted, which implys energy exchange occurs between these mechanical energy domains. The recovery between kinetic/potential and spring energy of nine participants is 59.7 ± 11.9 % as predicted from the leg model of this study (Table 3.6). This table also shows total net actuator work (ActNet), positive actuator work (ActPos), negative actuator work (ActNeg), total positive spring work (ElaPos) for the nine participants of Table A.1. ActNet, ActPos, ActNeg, and ElaPos are made dimensionless by normalizing by body weight and leg length. Comparing with the values in the previous optimization results (shown in Table 2.2.1), the multi-objetive optimization results in much

smaller value of ActNeg, while other values are slightly smaller than that of the previous optimization. This is because the previous optimization considers only positive mechanical work done by three force sources, and does not condiser any metabolic energy consumption of the negative and isometric mechanical work. In this model, metabolic energy comsumption of negative work of CE is a part of metabolic COT, and the optimizer finds such low ActNeg.

3.2.5 Model series-elastic unit activations and muscle EMGs

Figures 3-12 (a), (b), and (c) show average power curves of the participants 1 for each unit along with corresponding muscle EMGs from the literature [27]. At the ankle joint, in Figure 5 (a), the tibialis anterior (TA), gastrocnemius (GAS) and soleus (SOL) generate the torque. TA is activated at the early stance phase to impede ankle plantar flexion, and during the swing phase to keep the ankle angle at the reference $\hat{\theta}^a$ for preparation of the HS. GAS and SOL work from the mid stance phase to terminal stance to actively plantarflex the ankle. This is the same behavior exhibited by the ankle dorsiflexor and the ankle-knee biarticular unit in the model.

As Figure 3-12 (b) shows, the vastus muscle (VAS), gactrocnemius (GAS), bicep femoris short head (BFsh), rectus femoris (RF) and hamstrings (HAM) are attached at the knee joint. VAS operates as a monoarticular knee extensor during the early stance phase. The knee extensor in the model acts in a similar manner to the VAS. The GAS is a flexor for the knee joint and it is activated at mid stance phase. The GAS works to flex the knee at the mid stance phase. The BFsh flexes the knee joint at the terminal swing phase and the early stance phase. The model's knee flexor performs a similar function.

The knee-hip anterior is a biarticular unit and therefore affects the hip joint as well. As Figure 3-12 (c) shows, the knee-hip anterior also flexes the hip joint at the terminal stance phase and early swing phase. This indicates that the stored energy at the knee joint is transferrd, and then reused to flex the hip joint. Therefore, the knee-hip anterior unit in the model works in a similar manner to the RF. The knee-hip posterior is also a biarticular unit. However, this unit does little work at the hip

joint, while contribute a little at the late swing and early stance phase at the knee joint. This indicates this unit does transfer little mechanical energy, and the stored energy at the knee joint is return to the knee joint.

For the monoarticular hip muscle, the human leg comprises the iliopsoas (IL) and Gluteus maximus (GMAX), which act as a hip flexor and extensor, respectively. These muscles simply flex and extend the hip joint during walking, as do the model's hip flexor and extensor monoarticular units.

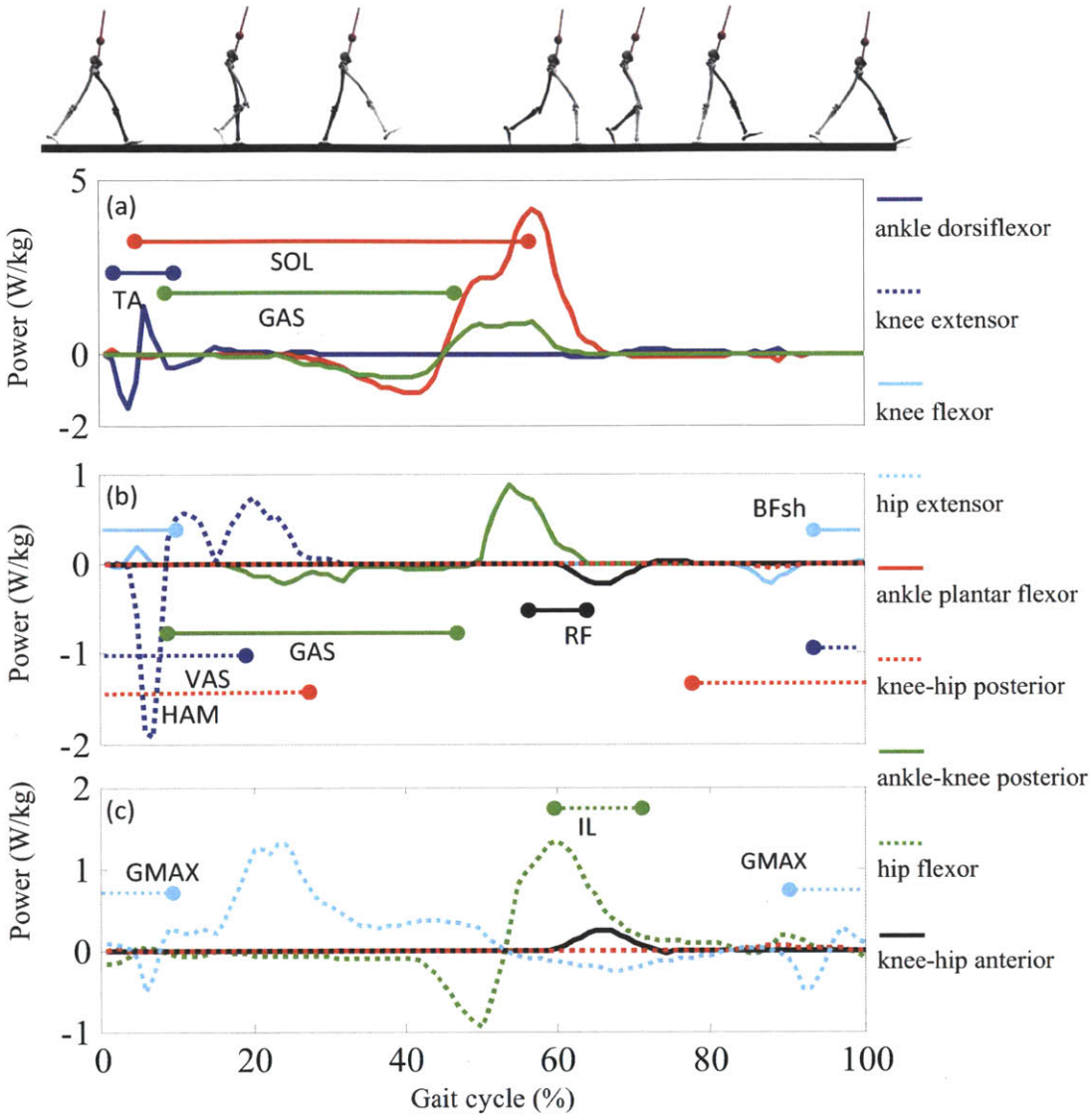

Figure 3-12: Spring contribution and EMG

Spring contribution power curves and muscle EMG for (a) ankle, (b) knee and (c) hip joints of one representative participant (Participant 1 in Table A.1). All Power curves also indicate periods when clutches, actuators or variable damper are activated. Muscle EMGs are shown as horizontal solid lines with two circles at the edges. (Tibial anterior (TA), soleus (SOL), vastus mucles (VAS), gastocnemius (GAS), hamstrings (HAM), bicep femoris short head (BFsh), rectus femoris (RF), glutus maximus (GMAX) and iliopsoas (IL)) EMG lines have the same color as the power curves that are anatomically and functionally equivalent.

3.2.6 Reflex dynamics of the ankle plantar flexor

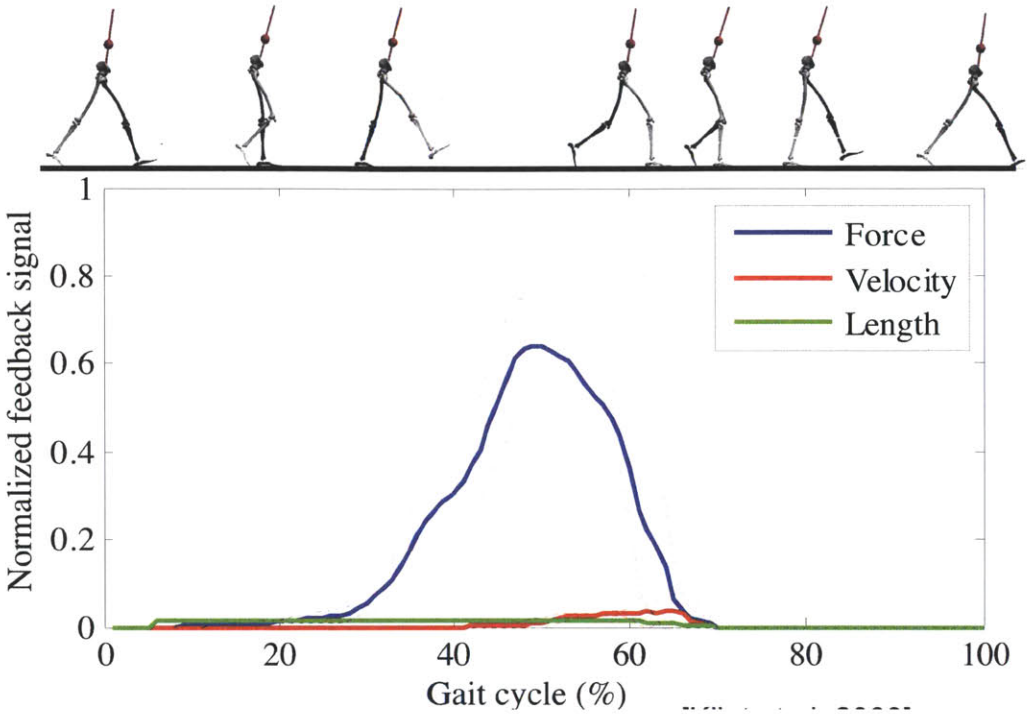

Figure 3-13: Feedback contribution of the ankle plantar flexor
The force, length and velocity feedback signal for the ankle plantar flexor of one representative participant (Participant 1 in Table A.1). The blue, red and green curves are force, velocity and length components of feedback signal. The data are the average of 10 steps in the steady state and dotted lines are one standard deviation from the average.

Figure 3-13 shows feedback signals from the ankle plantar flexor force, velocity, and length of one representative participant (participant 1 in Table A.1). The signals are the average of 10 steps of steady state during the stance phase. In the middle of the stance phase, the force feedback sharply increases, while the feedback signal from length is quite small, and the velocity feedback is zero. At the terminal stance phase, the velocity feedback signal increases a little which generates the ankle terminal plantar flexion.

The previous works also shows the similar trend. The positive force feedback term that dominates force production in our model was based on the studies of Geyer and Herr [21] and Prochazka et al. [47]. Notably, Klint et al. [3] isolated the contributions

of force-based and length-based afferent feedback during different intervals of stance at self-selected walking speed. They found that force feedback was dominant in late stance but contributed little during midstance perturbations, where spindle-based feedback probably dominates. This sequence is similar to that seen in my ankle plantar flexer reflex, although my modelling is done without perturbations. The further investigation with perturbation in the forward dynamics simulation would find how the length-based reflex work to stabilize the locomotion.

3.3 Discussions

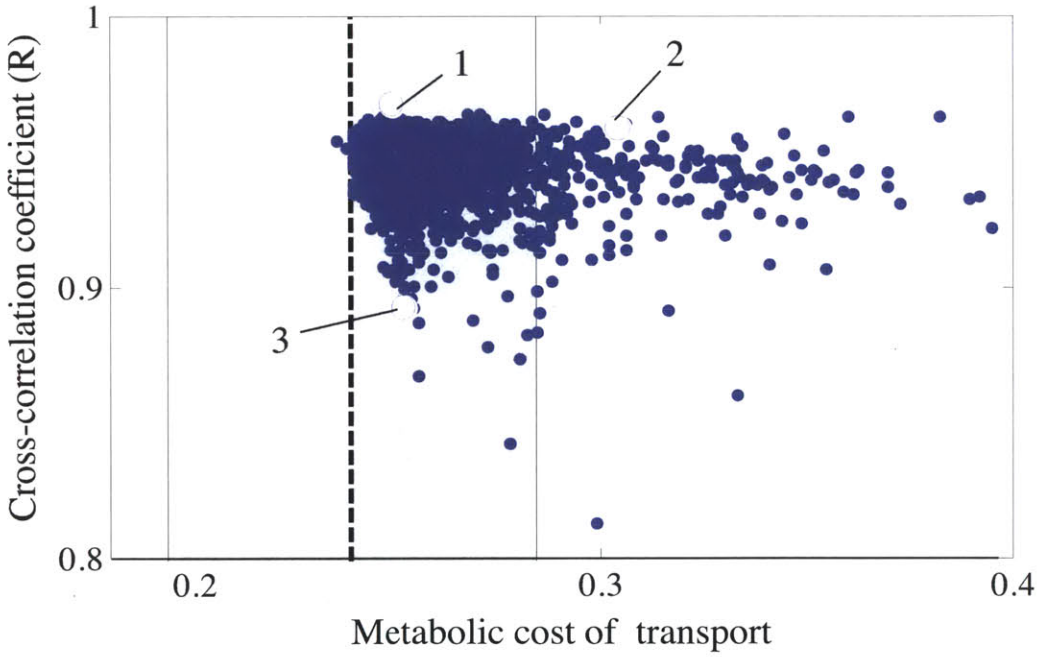

Figure 3-14: Relationship between metabolic COT vs R for a comparison study Each blue dots are individuals which can walk at least for 20 seconds in the forward dynamics simulation of the one representative participant (Participant 1 in Table A.1). The dashed line and shaded area is the average of human metabolic COT and the range within one standard deviation from the average [24]. In addition to the optimal solution (individual 1), an individuals with high R values 2, and another with low metabolic COT 3 are chosen for a comparison study.

	AP	HF	HE	KE	KHP	KF	KHA	AKP	AD
1	0.060	0.012	0.020	0.009	0.001	0.002	0.001	0.015	0.007
2	0.069	0.013	0.020	0.012	0.001	0.005	0.001	0.014	0.006
3	0.057	0.012	0.023	0.009	0.001	0.002	0.001	0.014	0.007

Table 3.7: Each unit contribution of metabolic COT
Each unit metabolic COT contribution of the ankle plantar flexor (AP), hip flexor (HF), hip extensor (HE), knee extensor (KE), knee-hip posterior (KHP), knee flexor (KF), knee-hip anterior (KHA), ankle-knee posterior (AKP) and ankle dorsiflexor (AD) of the left leg. These numbers are defined as the positive mechanical work done by a unit normalized by body weight and walking distance.

	R^a_{angle}	R^k_{angle}	R^h_{angle}
1	0.95	0.99	0.96
2	0.94	0.98	0.95
3	0.78	0.97	0.93

Table 3.8: Cross-correlation of each joint for a comparison study
R value breakdown of the individuals shown in Figure 3-14. R^a_{angle}, R^k_{angle}, and R^h_{angle} are cross-correlation coefficients of ankle, knee and hip joint angle.

3.3.1 Optimal versus non-optimal walking solution

I picked one individual as the optimal solution from Figure 3-5. As NSGA-II maintains a divergence of solutions for various combinations of metbaolic COT and R, looking at other individuals is useful to investigate what makes the model more biomechanical and economical. A comparison study of three different individuals from Figure 3-5 is conducted in this section.

I chose three different individuals among the optimization solutions of the one representative participant (participant 1 in Table A.1), and asigned the numbers as shown in Figure 3-14. The dashed line is the average of human metabolic COT and shaded area is the range of one standard deviation from the average [24]. The individual 1 is the optimal solution. The individual 1, and 2 have high R but different metabolic COTs. The individuals 1, and 3 have low values of metabolic COT, while they have different R values.

Table 3.7 shows metabolic COT contribution of the ankle plantar flexor (AP), hip flexor (HF), hip extensor (HE), knee extensor (KE), knee-hip posterior (KHP),

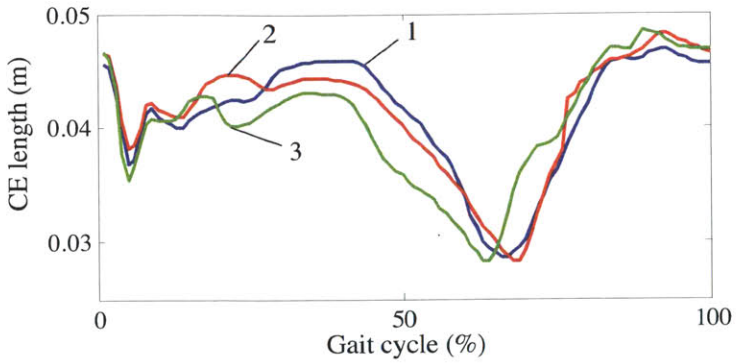

Figure 3-15: Length change of contractile element of the ankle plantar flexor
The CE length change of the ankle plantar flexor during one gait cycle of the individual 1, 2 and 3 in Figure 3-14. the data starts from the HS and ends at the next HS of the same leg. The blue, green and red curves are CE length change of the individual 1, 2 and 3, respectively.

knee flexor (KF), knee-hip anterior (KHA), ankle-knee posterior (AKP) and ankle dorsiflexor (AD) of the left leg. Each unit metabolic COT contribution is defined by metabolic energy expenditure normalized by body weight and walking distance. It turns out that the AP and KF of the individual 2 uses more metabolic energy than the individual 1, and the AP and HE of the individual 3 uses more and less metabolic energy, respectively than the individual 1. The other metabolic COT contributions of all individuals do not show significant difference.

Figure 3-15 shows the CE length change of the AP of the individual 1, 2 and 3 in one gait cycle. the data starts from the HS and ends at the next HS of the same leg. The CE of all individuals is stretched until the mid stance phase and then shortened at the terminal stance phase. The CE of the individual 1 is stretched most, and this indicates this muscle CE has larger eccentric behavior than other two and then concentric behavior with quick contraction at the terminal stance phase. As mention in the previous chapter, when a muscle is stretching (eccentric: $v_{CE} \geq 0$) or isometric($v_{CE} = 0$), metabolic power is relatively low. However, once a muscle starts to contract (concentric: $v < 0$), metabolic power increases sharply [34]. These data indicates the CE length change of the individual 1 needs less metabolic energy than the individual 2. The AP metabolic COT contribution of the individual 3 is smaller

	SE stiffness of AP (N/m)	SE stiffness of AKP (N/m)
1	251,120	40,783
2	248,850	41,145
3	247,069	42,106

Table 3.9: SE stiffness of the ankle plantar flexor and ankle-hip posterior
SE stiffness of the ankle plantar flexor (AP) and ankle-hip posterior (AKP)

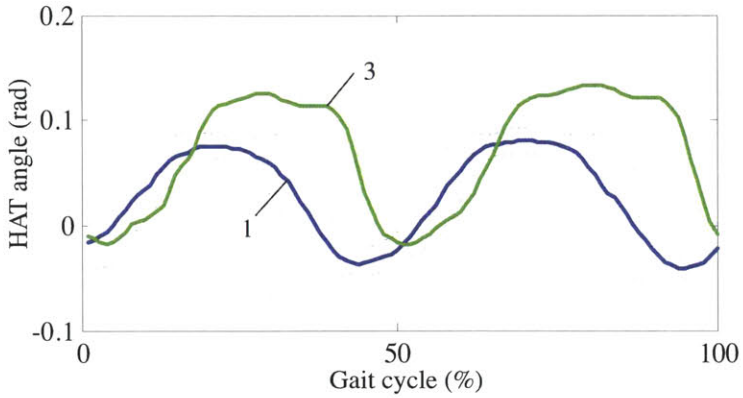

Figure 3-16: HAT segment angle
The HAT segment angle θ_{HAT} change durig one gait cycle of the individual 1 and 3 in Figure 3-14. the data starts from the HS and ends at the next HS of the same leg. The blue, and green curves are the HAT segement angle of the individual 1, and 3, respectively.

than the other, as its CE does stretch and contract less than the other two solutions do.

Table 3.9 shows the SE stiffness of the ankle plantar flexor and ankle-knee posterior. The SE of the ankle plantar flexor of the individual 1 is stiffer than the individual 2 and 3, while the SE of the ankle-knee posterior is less stiff than the others. Each CE length changes differently, because the SE stiffness is different, which results in different metabolic energy expenditure.

Table 3.8 shows each joint value of R. Only R^a_{angle} of individual 1 and 3 are significantly different, while the other values are not. These data indicates that difference on the AP and HE metabolic COT contribution dramatically reduces the R^a_{angle}, while the total metabolic COT is kept low. Figure 3-16 shows the HAT segment angle θ_{HAT} of the individual 1 and 2 with regard to the global axis. This

figure shows, the individual 2 walks leaning forward more than the individual 1. This walking behavior changes the contribution of muscles and breaks agreement on human biomechanics.

In summary,

- the SE stiffness and CE length change of the ankle plantar flexor correlate metabolic COT, and
- the ankle and hip muscle contributions correlate model's agreement with human biomechanics (but keeping low metabolic COT comparable with humans).

3.3.2 Mechanical efficiency in walking

Traditionally, the mechanical efficiency [41] has been used to evaluate a moving object as well as energetic and mechanical COT. The mechanical efficiency is calculated by the mechanical COT devided by the metabolic COT. As there are multiple definitions of mechanical COT, the values of mechanical efficiency varies.

Donelan et al. [14] measured human walking metabolic energy expenditure and mechanical work done by GRF, and estimate the effeciency of walking. The efficiency is defined by

$$\text{efficiency}_1 = -\frac{W^-_{GRF}}{E} \tag{3.15}$$

where W^-_{GRF} is the negative mechanical work done by GRF against the CM, and E is the total metabolic energy expenditure [14]. In the report, human is considered to walk with 0.25 of the efficiency. My model shows 0.22 of the efficiency with this definition (Participant 1 in Table A.1). However, mechanical COT calculated from GRF and CM position includes contribution of internal mechanical work, elasticity as well as actual muscle actuation.

Umberger and Martin [57] examined the influence of walking stride rate on efficiency using joint mechanical work. They defined the efficiency as follows:

$$\text{efficiency}_2 = \frac{W^+_{joint}}{E - W^-_{joint}} \tag{3.16}$$

where W_i^+ and W_i^- are the total positive and negative mechanical work of the all joints. The negative mechanical work is also considered as the negative work has the potential ot be returned as positive work later in the gait cycle [7]. Umberger and Martin results showed that when walking at 1.3 m, subjects had the efficiency of 0.38. Neptune et al. [50] constructed the musculoskeletal model for the self-selected speed walking with dynamics programming, and calculated the mechanical work of each joint and the mechanical efficiency using the same metabolic cost as Umberger and Martin used. The results showed the simulation has the similar efficiency (~ 0.40). My model shows 0.35 of the efficiency with this definition (Participant 1 in Table A.1). However, W_i^+ and W_i^- include contributions of elasticity as well as actual muscle mechanical work.

Recently, a few researchs on musculoskeletal models with a mathmatical muscle model enabled estimation of the mechanical efficiency from muscle contractile element defined by

$$\text{efficiency}_3 = \frac{W_{CE}^+}{E} \tag{3.17}$$

where W_{CE}^+ is positive mechanical work done by all contractile elements. Note that negative work does not need to be included in the denominator as the theoretical upper limit for how much elastic energy could be returned as positive work later in the gait cycle because the model could extract the CE work directly from the simulation. Neptune et al. [41] estimated an efficiency of 0.59 using the same metabolic cost as Umberger and Martine. On the contrary, my model shows the mechanical efficiency of 0.14 ± 0.01 for nine participants in Table A.1 using the metabolic cost calculated from my model. this number is much smaller than Neptune's, because I used an SEC as a muscle model except for the ankle plantar flexor, hip extensor and flexor, which always generates zero mechanical work. The optimizer minimized the positive mechanical work of the CEs of muscle models, which results in comparable metabolic COT. If I used Hill-type muscles instead of SECs, and if they generated more positive mechanical work, the model would not be able to walk with such low metabolic COT. This might be a reason why Neptune et al. adopted Umberger's metabolic cost instead

of calculating it from their own musculoskeletal model. However, in order to justify my model, further investigation on measuring muscle state is needed.

3.4 Energetics of SEC

An MTU is modeled as an SEC, as muscle CE energetics shows metabolic cost is quite low when muscle is isometric or eccentric. However, instead of isometric muscle model, a combination of eccentric and concentric CE motion with optimized SEE could be more economical (See Appendix B). In this section, metabolic cost of each SEC in the musculoskeletal model is minimized by replacing it with simple Hill-type muscle model as shown in Figure B-1. The force and CE length are obtained from the result of forward dynaamics simulation, and SEE stiffness is optimized such that metabolic cost of CE is minimized. Like the forward dynamics simulation, muscle biological parameters such as maximum force, maximum velocigy, optimal length of muscle fascicle are employed from literatures [21].

The result of each muscle unit optimization is shown in Table 3.10. The optimization shows slightly higher stiffness (1.05~1.18) and lower metabolic COT contribution (0.58~0.99) for all components. The numbers are normalized by the optimization result of NSGA-II (The best Solution in Table 3-14). The total metabolic COT for walking is 0.24, while the results of NSGA-II results in 0.25 of metabolic COT. This results indicates that, using SEA instead of SEC does not show significant difference and SEC is reasonable representation for a muscle model

Muscle unit	KE	KHP	KF	KHA	AKP	AD
SEE stiffness	1.17	1.14	1.13	1.21	1.05	1.18
Metabolic COT contribution	0.95	0.63	0.79	0.58	0.73	0.99

Table 3.10: Reoptimizaed SEE stiffness and metabolic COT contribution of each musle unit
Each unit optimized stiffness and metabolic COT contribution of the knee extensor (KE), knee-hip posterior (KHP), knee flexor (KF), knee-hip anterior (KHA), ankle-knee posterior (AKP) and ankle dorsiflexor (AD) of the left leg of the one representative participant (Participant 1 in Table A.1). The numbers are normalized by the optimization result of NSGA-II (The best Solution in Table 3-14).

Chapter 4

Conclusion and future Work

4.1 Thesis contribution

As I mentioned in the introduction chapter, human has more versatility on biped walking behavior than any kind for biped walking robots, and capability of walking as low energetic COT as biped walking robots based on passive dynamics. A key challenge is to understand how humans accomplish these features. The work accomplished in this thesis is (1)built a simple musculoskeletal architecture and investigate its energetics and role of elasticity with the optimization scheme, and (2)developed a neuro-musculoskeletal with Hill-type muscle model, and showed the model can walk as economically as human with human joint and torque biomechanics. These contributions can be further elaborated as follows:

4.1.1 Musculoskeletal architecture development

I hypothesize that quasi-passive, SEC units spanning the knee joint in a musculoskeletal arrangement can capture the dominant mechanical behaviors of the human knee in level-ground walking, and the musculoskeletal model was built with only three SEAs and SEC. The components around the knee joint were only quasi-passive elements.By cramping each joint to measured biological human walking joint angle, I optimized spring coefficients minimizing the error of the knee torque as well as mechanical COT

of three SEA. As a result, the model shows

- good agreement with biological knee joint.
- as low mechanical COT as humans
- a significant energy transfer from the knee to hip joint
- high %REC value of mechanical energy between kinetic, potential and elastic domain

4.1.2 Forward dynamics simulation of the model

By replacing SEAs with Hill-type muscle models, the neuro-musculoskeletal model was developed. As a controller of ankle and hip muscles, I employed simple reflex architecture, force, length and velocity feedback for the ankle plantarflexor, and PD controller of HAT or thigh segments for the hip extensor and flexor. I used an non-dominant sorting genetic algorithm (NGSA-II) to minimize metabolic COT as well as maximizing the agreement of joint kinematics with biological data. As a result, the model showed

- as low metabolic COT as human walking
- a good agreement on ankle, knee and hip joint kinematics
- high %REC value of energy between kinetic/potential and elasticity domain
- in the ankle plantarflexor, the force feedback is dominant, especially at the terminal stance phase, while in the early stance phase, the length feedback contributes more.

In particular, this model is the first ever that achieves as low metabolic COT as humans with a good agreement on human joint kinematics.

4.2 Future work

4.2.1 Comprehensive work on simulation model

The proposed model shows a great agreement on joint kinematics and metabolic COT with human at the self-selected walking speed. The model can be extended to fast and slow walking speed for comprehensive investigation. With regard to the feedback controller of the ankle plantar flexor, the length and velocity-related as well as the force-related feedback can be more investigated by perturbing the walking behavior. Finally by adding more SECs and Hill-type muscles, the model can be extended to the 3D model.

4.2.2 Hardware implication

The model motivates the new design paradigm of assistive robotic devices. As a preliminary application, I have already developed a transtibial prosthesis, which is composed of a powered ankle-foot prosthesis develop by iWalk [2] and an artificial gastrocnemius based on the model. A transtibial amputee usually does not have a functional gastrocnemius. The artificial gastrocnemius is an SEC spanning at the knee joint to generate the flexion torque in replacement of actual gastrocnemius. With this device, improvement on amputees' walking biomechanics is expected. In near future, clinical assessment and large scale clinical study will be conducted.

Appendix A

Human kinetic and kinematic data collection

Biological data including kinetic and kinematic walking information were collected at the Gait Laboratory of Spaulding Rehabilitation Hospital, Harvard Medical School, in a study approved by the Spaulding committee on the Use of Humans as Experimental Participants. Nine healthy adult participants, four male and five female, with an age range from 21 to 36 years, volunteered for the study. The participants walked at a self-selected speed across a 10 meter walkway in the Motion Analysis Laboratory. Participants were timed between two fixed points to ensure that the same walking speed was used between experimental trials. Walking speeds within a $\pm 5\%$ interval about the average self-selected speed were. Body mass, self-selected walking speed, center of mass (CM) height and leg length (L_{leg}) of each participant are shown in Table A.1. CM height was measured with equation (2.11), and leg length was measured as the vertical distance from the ground to the hip joint, when participants statically stand on the ground. For each study participant, a total of six walking trials were collected. The data collection procedures were based on standard techniques [29, 30, 32, 33] An infrared camera system (eight cameras, VICON 512 motion analysis system, Oxford Metrics, Oxford, UK) was used to measure the three-dimensional locations of reflective markers at 120 frames per second. A total of 33 markers were placed on various parts of a participant's body: 16 lower-body markers, five trunk

markers, eight upper-limb markers and four head markers. The markers were attached to the following bony landmarks: bilateral anterior superior iliac spines, posterior superior iliac spines, lateral femoral condyles, lateral malleoli, forefeet and heels. Additional markers were rigidly attached to wands over the mid-femur and mid-shaft of the tibia. The kinematics of the upper body were also collected with markers placed on the following locations: sternum, clavicle, C7 vertebra, T10 vertebra, head, and bilaterally on the shoulder, elbow and wrist. The VICON 512 system was able to detect marker position with a precision of 1 millimeter. During the walking trials, ground reaction forces were measured synchronously with the kinematic data at a sampling rate of 1080 Hz using two staggered force platforms (model no. 2222 or OR6-5-1, Advanced Mechanical Technology Inc., Watertown, MA, USA) embedded in the walkway. The platforms measured ground reaction force and center of pressure location at precisions of ~0.1N and ~2mm, respectively. Joint torques and powers were then calculated using a standard inverse dynamics model (Vicon Bodybuilder; Oxford Metrics, UK) and were normalized for body weight. Prior to modeling and analysis, all marker position data was low pass filtered using a 4th order digital Butterworth filter at a cutoff frequency of 8 Hz. This filter frequency was based on the maximum frequency obtained from a residual analysis of all marker position data, and processed as one whole gait cycle with 100 discrete data points from the heel strike to the next heel strike of the same leg.

Participant	M (kg)	V_{self} (m/s)	H_{cm} (m)	L_{leg} (m)
1	81.9	1.32	1.08	0.99
2	57.2	1.40	0.92	0.90
3	82.6	1.24	1.08	0.88
4	65.3	1.18	0.99	0.88
5	50.1	1.30	0.88	0.75
6	64.6	1.41	1.03	0.91
7	73.9	1.18	1.01	0.89
8	49.9	1.06	0.88	0.75
9	62.7	1.38	0.94	0.81
mean	65.3	1.27	0.98	0.86
±s.d.	12.2	0.12	0.08	0.08

Table A.1: Participant information
Body mass M, self-selected walking speed V_{self}, CM height H_{cm} and leg length L_{leg} of each study participant

Appendix B

Muscle model energetics

In this thesis, I hypothesize that

- quasi-passive, SEC units spanning the knee joint in a musculoskeletal arrangement can capture the dominant mechanical behaviors of the human knee in level-ground walking,
- since an SEC is incapable of dissipating mechanical energy as heat, a corollary to this hypothesis is that such a quasi-passive robotic knee would necessarily have to transfer energy via elastic biarticular mechanisms to hip and/or ankle joints, and
- such a transfer of energy would reduce the necessary actuator work to track human torque profiles at the hip and ankle, improving the mechanical economy of a human-like walking robot.

and I modeled a musculoskeletal knee joint only with SECs. Another advantage of this model is that hardware implementation can be done more easily than SEAs. Moreover, as Ma and Zahalak reported [34], metabolic cost of muscle contractile element is quite low when it is isometric and eccentric [34]. This report on muscle energetics supports my model as an SEC is one representative model of muscle isometric behavior. At the same time, this fact also implies that the muscle model could be more economical with combination of muscle eccentric and concentric motions than only isometric behavior.

In this chapter, I estimate muscle metabolic energy consumption of single Hill-type muscle with various SEE stiffness and investigate the most economical CE behavior.

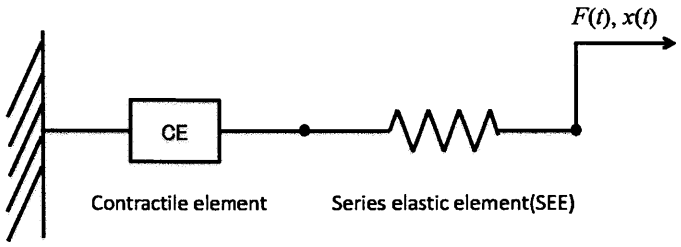

Figure B-1: Single Hill-type muscle model
A single muscle model with a contractile element and series elastic element. Its force $F(t)$ and length $x(t)$ are fixed.

B.1 Method

A Hill-type muscle model is shown as Figure B-1. This muscle model is composed of a contractile element (CE) and seris elastic element (SEE) in series. In this simulation, force $F(t)$ and length change $x(t)$ of total MTU are enforced. Under this condition, metabolic energy consumption of the CE is calculated once a stiffness of SEE is fixed. A procedure of calculating metabolic cost is as follows:

1. calculate length change and velocity of CE ($l_{CE}(t)$ and $v_{CE}(t)$).
2. calculate the muscle excitation with Equation 3.1
3. calculate metabolic power of CE using Equation 3.13.
4. and integrate the metabolc power over time t.

Here, three type of inputs are used which are combinations of simple sinusoidal waves with peeks at $T/4, T/2$ and $3T/4$ for length change $x(t)$ as shown in Figure B-2. These all inputs enforce the MTU stretch at first, contract and then return to the original position. Regarding to the force, I used a virtual linear spring force with linear stiffness k'. The force is calculated with

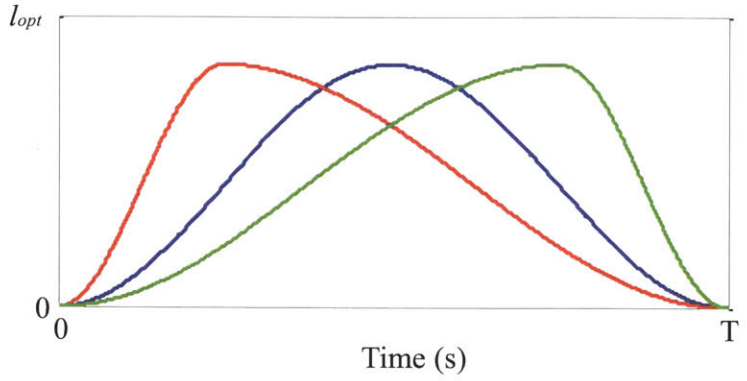

Figure B-2: Length change of MTU
Three kinds of length inputs are used. Red, blue and green curves have peaks at T/4, T/2, and 3T/4, respectively, where T is simulation duration ($T = 1s$). These all inputs enforce the MTU stretch at first to l_{opt}, contract and then return to the original position.

$$F(t) = k'x(t) \tag{B.1}$$

and if the SEE stiffness k is equivalent to k', the CE length would not change and only SEE would be streched and shortened through the simulation. Parameters of the Hill-type muscle are shown in Table B.1.

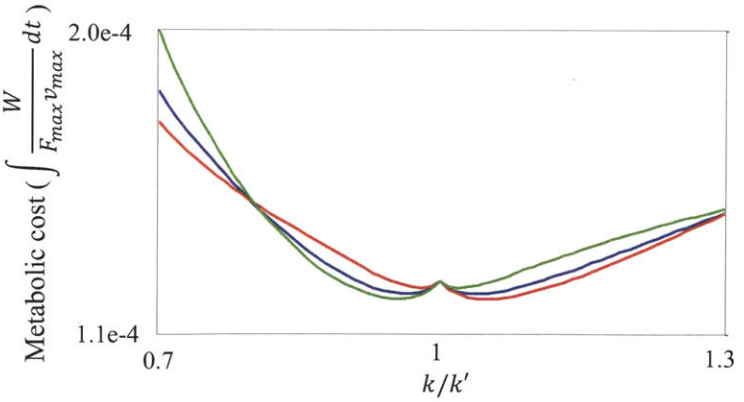

Figure B-3: Metabolic cost of single muscle model

Table B.1: Parameters for muscle model

Parameter	Description	Value
w	width of the bell shaped f-l curve	0.56
c	shape of bell shaped curve near the extremes of the bell	0.05
N	muscle force (in units of F_{max}) at maximum lengthening velocity $v_{CE} = v_{max}$	1.8
K	curvature constant	5
T	simulation duration(s)	1
l_{opt}	muscle fascicle optimal length(m)	0.1
v_{max}	muscle fascicle maximum velocity(m/s)	$6l_{opt}$

These parameters define the shape of the force-length and force-velocity function. The values are employed from [17].

B.2 Result

The metabolic cost for each length change and force are shown in Figure B-3. The color convention is same as Figure B-2. The metabolic cost and SEE stiffness are normalized by the product of maximum force and maximum velocity, and the virtual stiffness k', respectively. Each result shows two local minima where k/k' is slightly less and greater than 1. When k/k' is less than 1, the CEE length, at first, contracts and then streches, while the total MTU length streches at first, and then contracts. On the other hand, when k/k' is greater than 1, the CE length streaches and contracts, while the total MTU length contracts and then stretches. And when $k/k' = 1$, the CE length does not change and only SEE length streches and contracts.

From biomechanics constraint, it is reasonable to assume $k/k' \geq 1$, as motion of CE and total MTU are always in the same direction. The metabolic cost is not minimized at $k/k' = 1$, but the value is quite close to the minimam. For example, when $k/k' = 1$, all inputs result in the same value of the metabolic cost, 1.25E-4. On the other hand, The green, blue and red curves have the metabolic costs of 1.23E-4, 1.21E-4, and 1.20E-4 at their minima, respectively. So the difference are only 4% at most.This result indicates that it is reasonable enough to model a muscle with SEC in terms of energetics.

Appendix C

Hardware Implementation

A chapter 2 shows that the behavior of the gastrocnemius muscle can be mimicked by a spring and clutch in series. This result indicates that a mono knee flexor composed of only a clutch and linear spring should improve the walking behavior of transtibial amputees during walking. In this chapter, I first describe a musculoskeletal model of a transtibial amputee based on a full leg model shown as Figure 2-5 and then show a mechanical design of hardware.

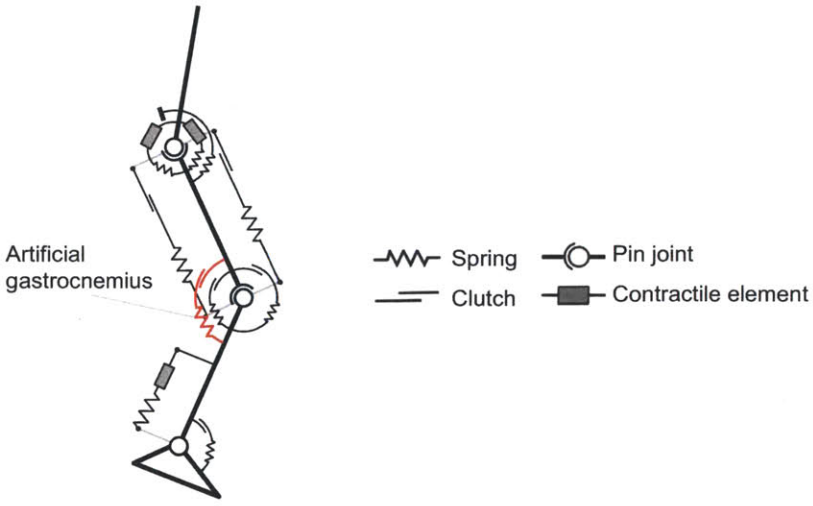

Figure C-1: Muscle metabolic power in steady-state
Musculoskeletal model of a transtibial amputee with a powered ankle-foot prosthesis and artificial gastrocnemius (AG) shown as a red component. The other knee and hip components are exactly same as a full musculoskeletal model shown in Figure 2-5.

C.1 Transtibial amputee model

C.1.1 Musculoskeletal model for a transtibial amputee

Figure C-1 shows a two-dimensional musculoskeletal leg model for a transtibial amputee composed of eight series-elastic clutch/actuator mechanisms. In the powered ankle-foot prosthesis at the ankle joint, a linear spring and actuator in series as well as a parallel spring are attached. In this study, I assume that the active component of the ankle joint allows it to mimic the behavior of the ankle foot complex and consequently perform an optimization only for the knee and hip joints. The hip extensor and flexor are active components with unidirectional actuators and the other units around the knee and hip joints are composed of clutches and springs. When a clutch is disengaged, the joint rotates without any resistance from spring. When a clutch is engaged, the clutch holds the series elastic spring at its current position and the spring begins to store energy as the joint rotates in a manner comparable to a muscle-tendon unit where the muscle generates force isometrically. The knee and hip joints are composed of five monoarticular and two biarticular tendon-like springs with series clutches or actuators. We assume that all monoarticular units are rotational springs and clutches while all biarticular units act about attached pulleys with fixed moment arm lengths.

C.1.2 Optimization

The model has a total of 12 series-elastic clutch parameters for the knee and hip joints: seven spring constants and five distinct times when clutches are engaged. These parameters and actuator movements define joint torque. Fitting this model to biomechanical data involved determining the spring rates of the model's seven springs and the engagement times of the five associated clutches. The biomechanical data for this procedure was obtained from nine participants shown in Table A.1.

An optimization procedure is used to fit the parameters of the model to the biomechanical data. I used the same strategy as shown in the chapter 2.

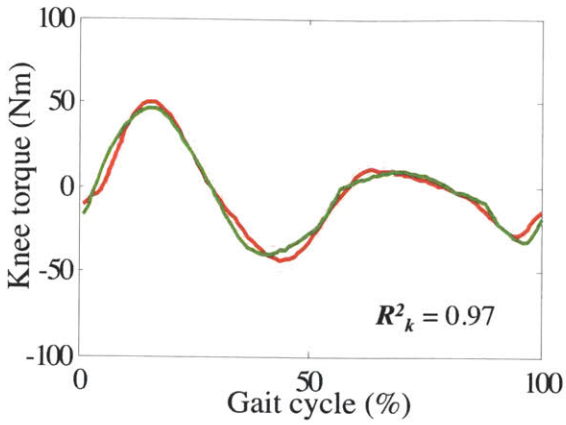

Figure C-2: Muscle metabolic power in steady-state
Knee torque of one representative perticipant (Paritic pant 1 of Table A.1)from the optimization result. Green and red curves are the result of the simulation and biological torque, respectively. Dotted curves are one standard deviation from the biological data.

C.1.3 Result

Figure C-2 shows the knee torques from the musculoskeletal model simulation and biological data of one representative participant (Participant 1 of Table A.1). Since R^2 is 0.96, I see that the gross features of human walking at self-selected speed may be captured using only quasi-passive elements including the AG. The knee torque agreement of other participants are shown in Table C.1. These optimizations show good agreement between biological and simulated knee torque for all participants (0.94 ± 0.03). This means a linear spring in series a clutch can contribute as a gastrocnemius for the knee joint at the self-selected walking speed. This result also suggests that optimized stiffness in seris a clutch would improve transtibial amputee walking behavior.

C.2 Hardware Configuration

To evaluate the viability of the model for the self-selected walking speed, the model is used to control a prosthetic apparatus comprising a powered ankle-foot prosthesis and an AG. The ankle and knee joint states are measured and used to provide real

Participant	R^2
1	0.97
2	0.94
3	0.97
4	0.94
5	0.87
6	0.92
7	0.93
8	0.95
9	0.97
mean	0.94
s.d.	$\pm$ 0.03

Table C.1: Knee torque agreement between simulation and bilogical data of all participants

time input to the neuromuscular model simulated by an on-board microcontroller. The resulting torque command from the neuromuscular model is used to produce ankle torque while a knee controller adjusted the torque produced by the knee brace. This configuration, shown in Figure C-3, is set up to enable the prosthetic apparatus to behave as if it were a human lower-leg with reflex-controlled muscles acting at the ankle.

C.2.1 Powered Ankle-Foot Prosthesis

This study makes use of a powered ankle-foot prosthesis (iWalk, LLC, Cambridge, MA [2]) having a similar size and weight (1.8 kg) to the intact biological ankle-foot complex. The prosthesis included a brushless motor, ballscrew transmission, and Kevlar leaf-spring that together comprised a series-elastic actuator (SEA) [46]. The SEA was capable of producing torque about the revolute ankle joint, analogous to the torque produced by the plantar flexor and dorsiflexor muscles about the human biological ankle joint. The ankles theoretical torque capability exceeded 300 Nm. A unidirectional parallel spring engaged when the ankle was dorsiflexed and thereby assisted the SEA during walking [6]. A compliant carbonfiber leaf-spring attached to the base of the prosthesis acted as a foot.

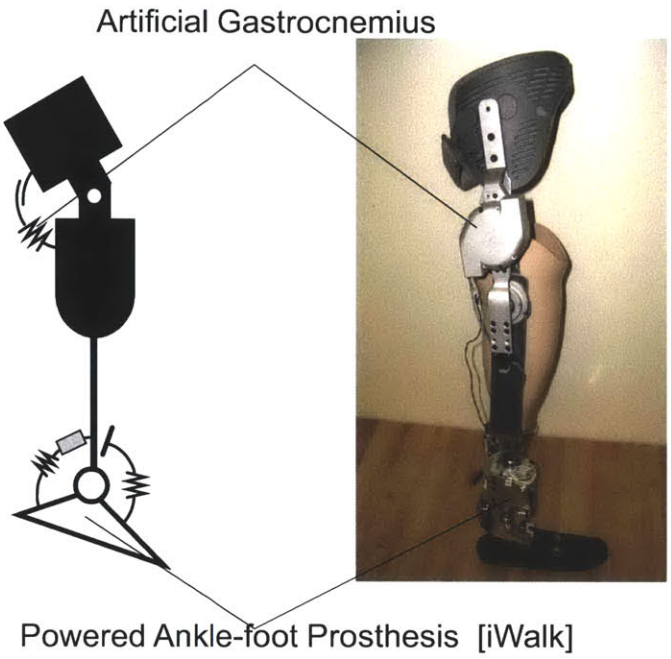

Figure C-3: Hardware configuration
A transibial prosthesis system includes a powered ankle-foot prosthesis developed by iWalk, LLC [2] and AG. An AG is embedded at the knee brace and generates torque for knee flexion. All electronics are attached in the ankle prosthesis and sensory information is collected at the real time.

C.2.2 Artificial Gastrocnemius

Since the AG are biarticular muscles and they act at both the ankle and knee, an AG is mounted at the knee brace to provide the knee flexion action of the gastrocnemius. A contribution of a gastrocmemius muscle for the ankle joint is emulated by the powered ankle-foot prosthesis. The AG mechanism consisted of a pair of dog gears at the free end of a coil spring (spring stiffness of 120 Nm/rad) which acted as a knee flexor on a polycentric knee brace. As the AG is composed of only quasi-passive elements, the size and weight is relatively small and light (0.47kg) comparing with other active devices. The brace was integrated into a prosthetic socket connected to the ankle-foot prosthesis. When the clutch was engaged via solenoid action, the free end of the spring locked with respect to the socket and the spring stretched as the knee straightened. The force developed by the spring produced a flexion torque at

the knee joint. Conversely, when the clutch disengaged no torque was applied at the knee joint.

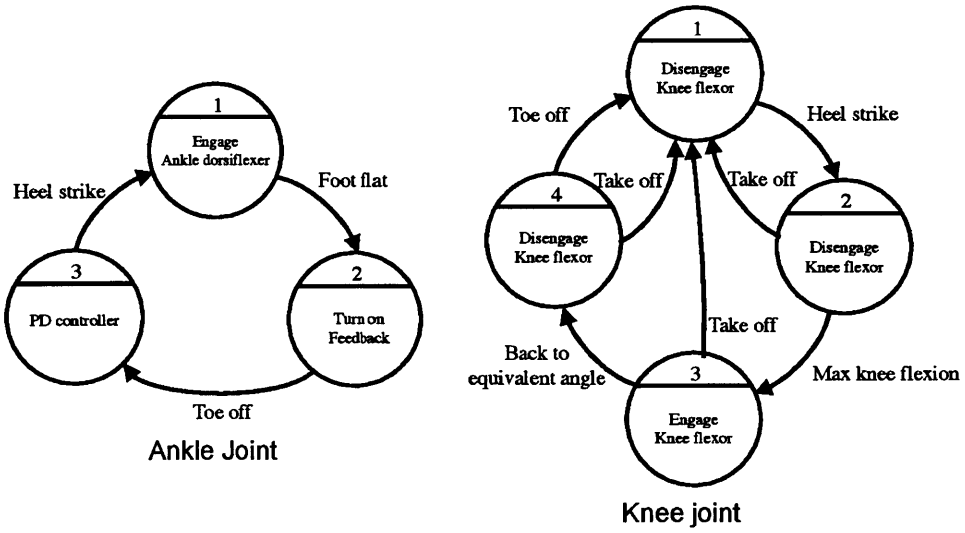

Figure C-4: Finite state machine

Ankle and knee joint state machines are constructed based on the method shown in the chapter 3. The ankle joint state machine includes three states which turns feedback control on only after foot flat during the stance phase. The knee joint state machine engages the clutch on only after the maximum knee flexion during the stance phase.

C.2.3 Controller

AG and powered ankle-foot prosthesis are controlled based on simple finite state machines shown in Figure C-4. The state machine for the ankle joint is exactly same as one used in forward dyanmics simulation in the chapter 3. This state machine turns the feedback control on only at time of foot flat during the stance phase. Force, length, and velocity feedback control are turn on at that time and gains and parameters are obtained from the optimization results.

The state machine for the AG is constructed based on an EMG signal from the gastrocnemius muscle [27] which is activated approximately from the maximum knee

flexion to toe off. This also matches with my model optimization shown in the chapter 2. The clutch is engaged at the time of the maximum knee flexion and then disengaged when the knee angle returns to the original postion of the spring.

C.3 Pilot clinical study

C.3.1 Method

As a pilot study, I tested this transtibial prosthesis on one subject (47yr, 1.72m, 88.5kg, right leg amputee). There are three conditions which are (1) walking with his own passive prosthesis (flexfoot), (2) walking with powered ankle-foot prosthesis with the AG off, and (3) walking with powered ankle-foot prosthesis with the AG on. Only steady-state gait cycles within 10 per cent of the target walking speed (1.25m/s) are used for analysis. I collect data of 10 trials per condition. For each walking trial, the participant began walking approximately 3 m from the beginning of the pathway and stopped walking approximately 3 m past the end of the path. The beginning and end of the 5.3 m path were labelled with markers on the ground. A stopwatch was used to verify the average walking speed for each trial by noting when the subject's centre of mass passed over each of the markers.

This clinical experiments were approved by MIT's Committee on the Use of Humans as Experimental Subjects (COUHES). After giving informed consent, a amputee participant is fitted with the prosthetic apparatus.

C.3.2 Result

Kinetics and Kinematics

Figure C-5 shows ankle angle of both legs. Intact ankle does not show significant difference among three conditions. On the other hand, affected ankle shows that powered ankle-foot prosthesis behaves more biomechanically. This is also seen in torque profile shown in Figure C-6. The powered ankle-foot prosthesis generates less torque during the mid of stance phase. This improvement helps the amputee's body

to propel forward. Mechanical net work of affected ankle is 0J, 16 ± 4J, 15 ± 5J for condition 1, 2 and 3, respectively, while mechanical net work of normal human ankle is 16J [23], the ankle joint generates enough mechanical energy for the normal walking speed.

The knee joint angle and torque are shown in Figure C-7 and C-8, respectively. Though knee angle does not show any significant difference between affected and intact leg as well as among three condition, intact knee torque shows that the robotic prosthesis contributes to decrease the knee extension torque at the maximum knee flexion during the stance phase. This is because the robotic ankle pushes off the ground, and this motion helps the body move forward and upward. However, there is no significant difference between two conditions with the powered ankle-foot prosthesis (2) and (3), even though the AG generates knee flexion torque.

The hip joint angle and torque are shown in Figure C-9 and C-10, respectively. Even though the powered ankle generates enough mechanical energy, there is no significant difference between intact and affected leg as well as among three conditions.

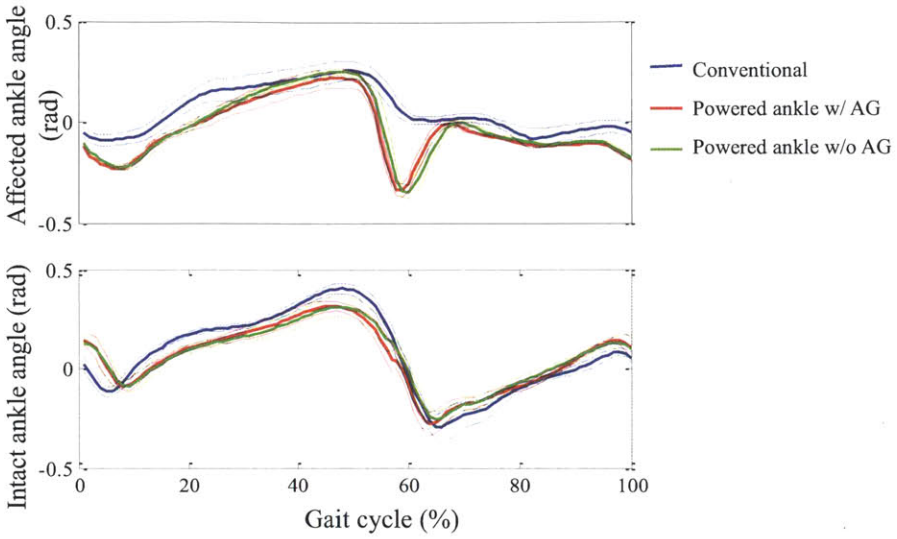

Figure C-5: Ankle angle

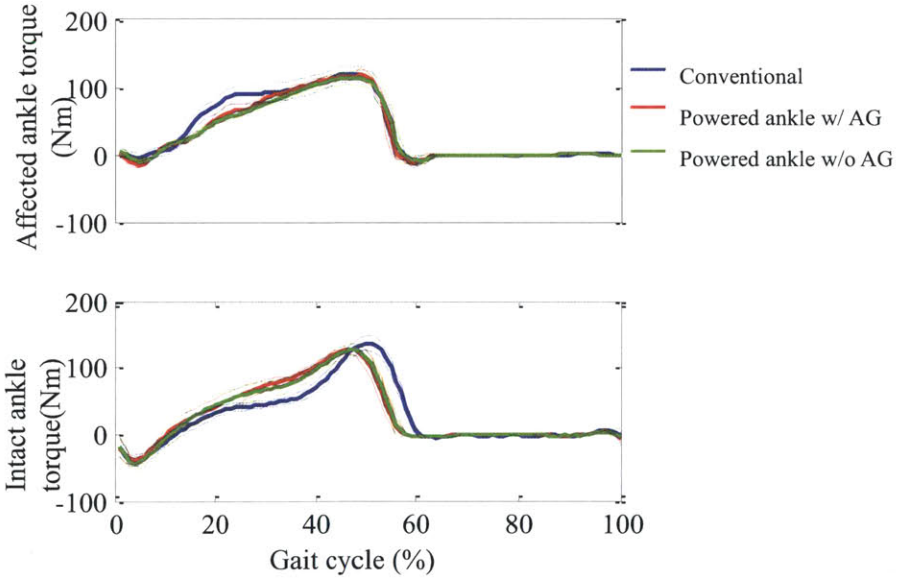

Figure C-6: Ankle torque

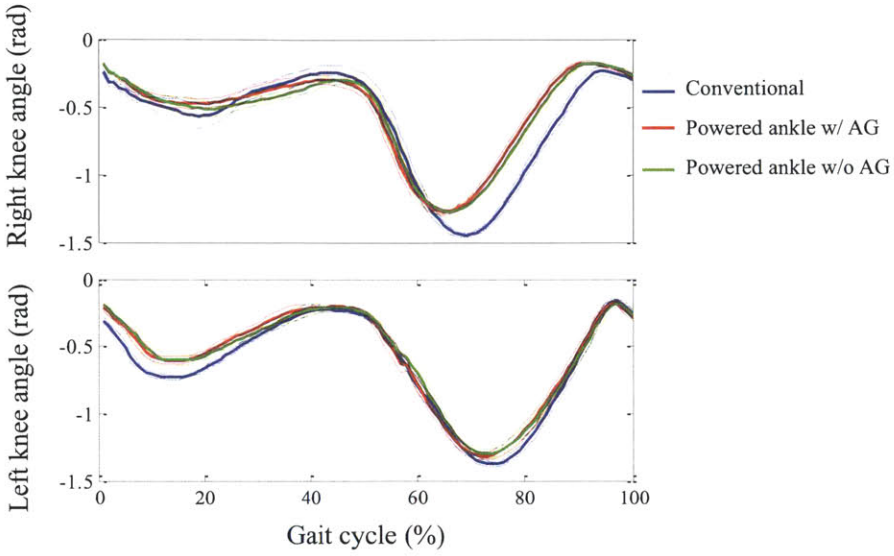

Figure C-7: Knee angle

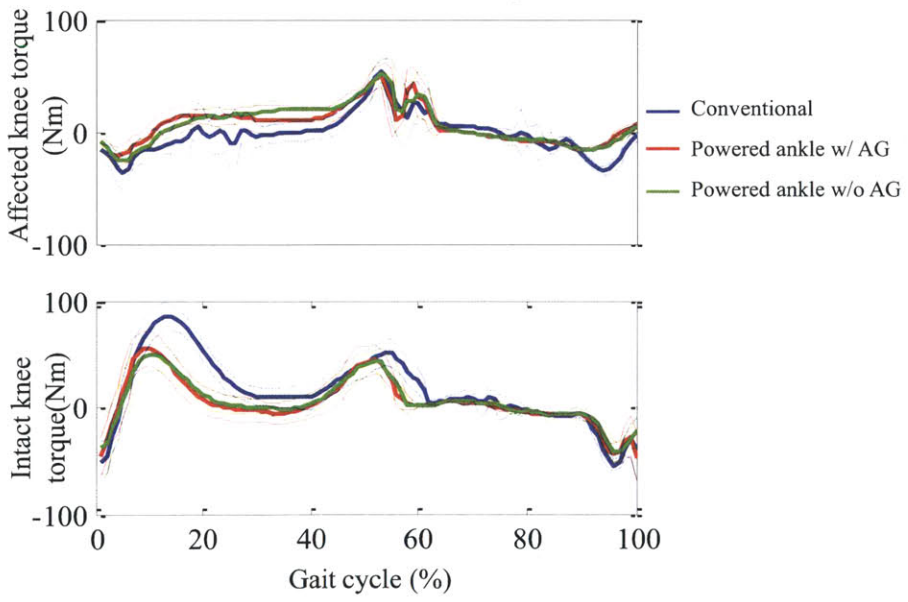

Figure C-8: Knee torque

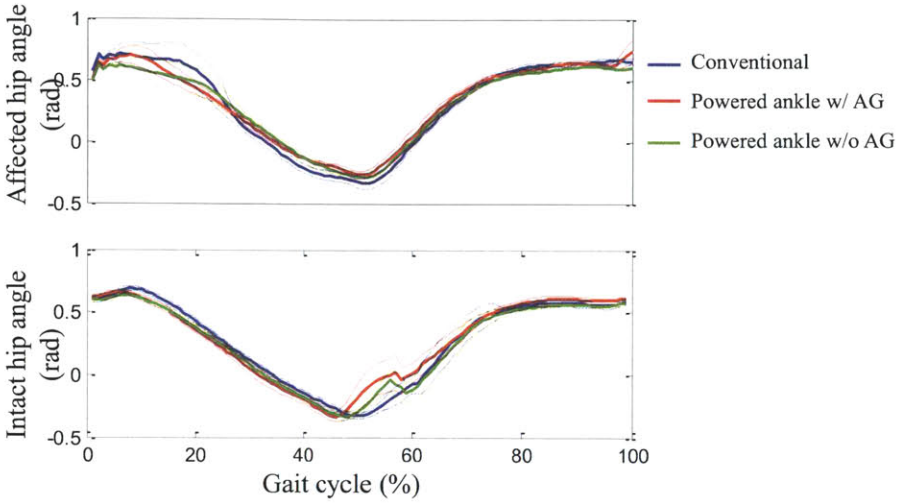

Figure C-9: Hip angle

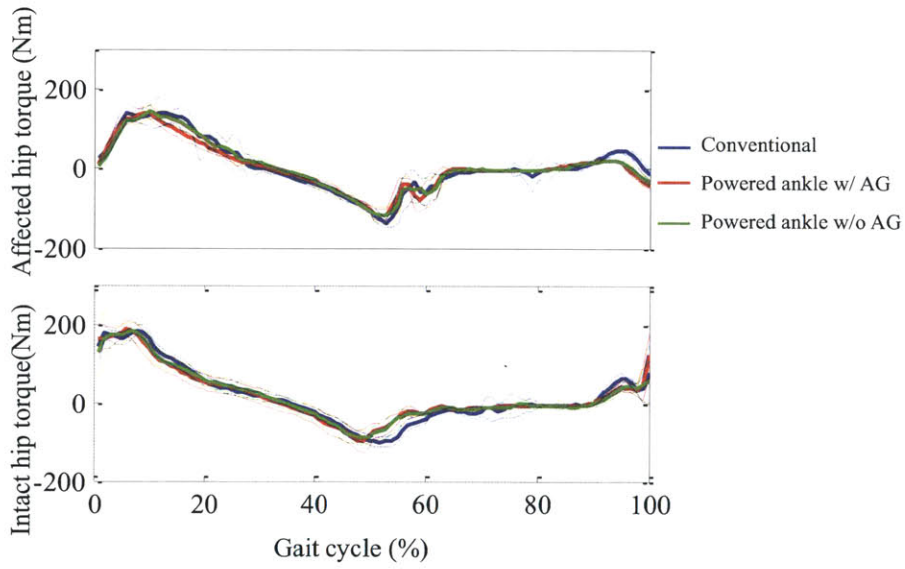

Figure C-10: Hip torque

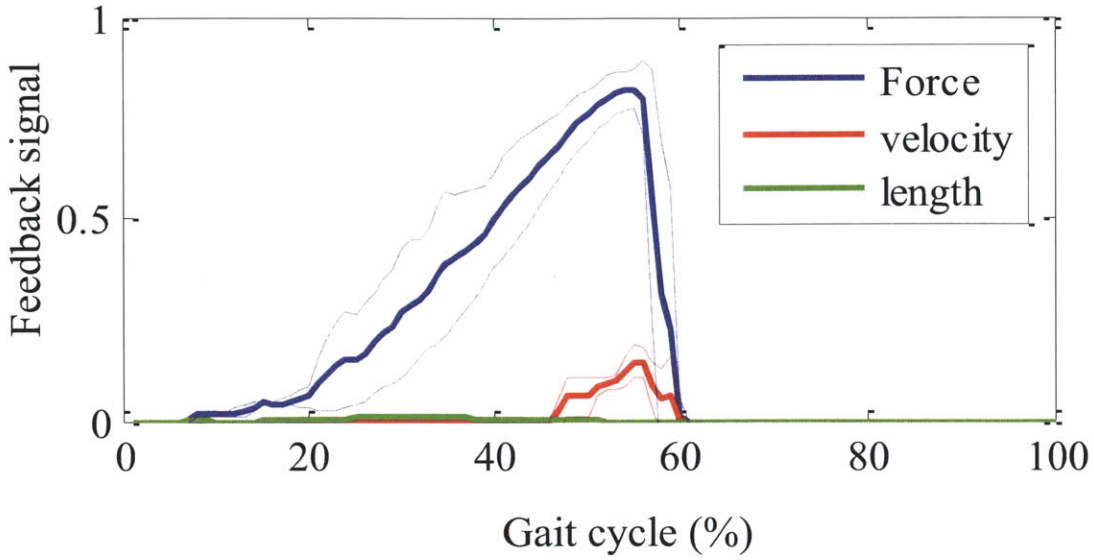

Figure C-11: Feedback signal

Feedback signals

The powered ankle-foot prosthesis emulates muscle behavior and its force, length and velocity feedback signal for the ankle plantar flexor is shown in the Figure C-11. The data are the average of 10 steps in the steady state and dotted lines are one standard deviation from the average. In the middle of the stance phase, the force feedback sharply increases, while the feedback signal from length is quite small, and the velocity feedback is zero. At the terminal stance phase, the velocity feedback signal increases a little which generates the ankle terminal plantar flexion. This is quite similar behavior which is seen in the forward dyanmics simulation (Figure 3-13)

C.3.3 Discussion

As shown above, unfortunately, I don't see any advantage of the AG while the powered ankle-foot prosthesis works well. Figure C-12 shows knee torque with the AG contribution. The biological knee joint torque of condition 2 and 3 with the AG contribution is illustrated. This plot indicates that the biological knee joint under

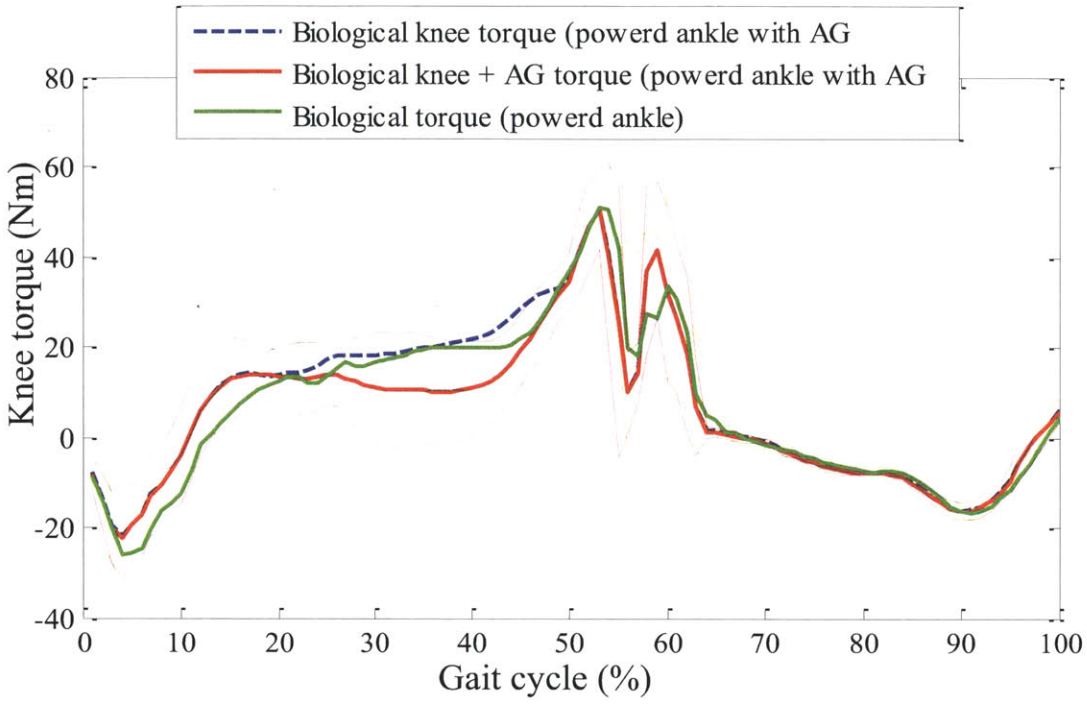

Figure C-12: Knee torque of affected leg and artificial gastrocnemius contribution

these two conditions behaves similarly and AG does not affect biological knee torque output. In the other word, human body generates original torque pattern when external torque is applied at the knee joint. This tendency is also seen in Elliott thesis [15]. This might be because that patient was not able to adapt a neuro reflex system. Human walking behavior is constructed mainly based on a neuro-reflex control system [21], which has been acquired usually over long period. Therefore, long term training may increase the walking biomechanics and metabolism. As the data only show output from one participant, further clinical study and investigation need to be done in the future.

Bibliography

[1] http://world.honda.com/ASIMO

[2] http://www.iwalkpro.com

[3] Richard af Klint, Jens Bo Nielsen, Jonathan Cole, Thomas Sinkjaer, and Michael J. Grey. Within-step modulation of leg muscle activity by afferent feedback in human walking. *The Journal of Phisiology*, 586(19):pp.4643–4648, 2008.

[4] Richard af Klint, Jens Bo Nielsen, Thomas Sinkjaer, and Michael J. Grey. Sudden drop in ground support produces force-related unload response in human overground walking. *J Neurophysiol*, 101:pp.1705–1712, 2009.

[5] Frank C. Anderson and Marcus G. Pandy. Dynamic optimization of human walking. *Journal of Biomechanical Engineering*, 123:pp.387–390, 2001.

[6] S. Au, P. Dilworth, and H. Herr. An ankle-foot emulation system for the study of human walking biomechanics. In *Proc. IEEE int. conf. on robotics and automation*, pages pp.2939–2945, 2006.

[7] Prilutsky BI. Work, energy expenditure, and efficiency of the stretchshortening cycle. *J. Appl. Biomech.*, 13(4):pp.466–70, 1997.

[8] G A Cavagna, H Thys, and A Zamboni. The sources of external work in level walking and running. *J. Physiol.'*, 262:pp.639–657, 1976.

[9] Steven Hartley Collins and Andy Ruina. A bipedal walking robot with efficient and human-like gait. *Proc. IEEE Int. Conf. Robotics and Automation*, 2005.

[10] Neil J. Cronin, Masaki Ishikawa, Michael J. Grey, Richard af Klint, Paavo V. Komi, Janne Avela, Thomas Sinkjaer, and Michael Voigt. Mechanical and neural stretch responses of the human soleus muscle at different walking speed. *J. Physiol*, 2009.

[11] K. Deb and T. Goel. A hybrid multi-objective evolutionary approach to engineering shape design. In *International Conference on Evolutionary Multi-Criterion Optimization (EMO-2001)*, pages pp.385–399, 2001.

[12] Kalyanmoy Deb and Deb Kalyanmoy. *Multi-Objective Optimization Using Evolutionary Algorithms*. Wiley, 2001.

[13] S. Delp. *A computer graphics system to analyze and design musculoskeletal reconstructions of the lower limb.* PhD thesis, Stanford, 1990.

[14] J. Maxwell Donelan, Rodger Kram, and Authur D. Kuo. Mechanical work for step-to-step transitions is a major determinant of the metabolic cost of human walking. *The Journal of Experimental Biology*, 205:pp.3717–3727, 2002.

[15] Grant Elliott. Design and evaluation of a quasi-passive robotic knee brace: On the effects of parallel elasticity on human running. Master's thesis, MIT, 2012.

[16] A.M. Wilson G.A. Lichtwark. Interactions between the human gastrocnemius muscle and the achilles tendon during incline, level and decline locomotion. *The Journal of Experimental Biology*, 209:pp.4379–4388, 2006.

[17] Blickhan R. Geyer H, Seyfarth A. Positive force feedback in bouncing gaits? *Proceedings of the Royal Society of London, Series B: Biological Science*, 270(1529):pp.2173–2183, 2003.

[18] M. J. Grey, J. B. Nielsen, N. Mazzaro, and T. Sinkjaer T. Positive force feedback in human walking. *Journal of Physiology*, 581(1):pp.99–105, 2007.

[19] D. Grieve, S. Pheasant, and P. Cavanagh. Prediction of gastrocnemius length from knee and ankle joint posture. *International series on biomechanics*, 2A:pp.405–412, 1978.

[20] Y. Y. Haimes, L. S. Lasdon, and D. A. Wismer. On a bicriterion formulation of the problems of integrated system identification and system optimization. *IEEE Transcations on Systems, Man, and Cybernetics*, 1(3):pp.296–297, 1971.

[21] Hugh Herr Hartmut Geyer. A muscle-reflex model that encodes principles of legged mechanics produces human walking dynamics and muscle activities. *IEEE Transaction on Neural Systems and Rehabilitation Engineering*, 18(3):263–273, 2010.

[22] K. Hase and N. Yamazaki. Computer simulation study of human locomotion with a three-dimensional entire-body neuro-musculo-skeletal model, i. acuisition of normal walking. *JSME Int. J., Series C*, 45(4):pp.1040–1050, 2002.

[23] H. Herr and M. Popovic M. Angular momentum in human walking. *Journal of Experimental Biology*, 211:pp.467–480, 2008.

[24] Hugh M. Herr and Alena M. Grabowski. Bionic ankle-foot prosthesis normalizes walking gait for persons with leg amputation. *Proceedings of the Royal Society B Biological Sciences*, 2011.

[25] A. V. Hill. The heat of shortening and the dynamic constants of muscle. *Proceedings of the Royal Society of London. Series B, Biological Sciences*, 126(843):pp.136–195, 1938.

[26] Masaki Ishikawa, Paavo V. Komi, Michae J. Grey, Vesa Lepola, and Gert-Peter Bruggemann. Muscle-tendon interaction and elastic energy usage in human walking. *J Appl Physiol*, 99:pp.603–608, 2005.

[27] Perry J. and Schoneberger B. *Gait Analysis: Normal and Pathological Function.* SLACK incorporated, 1992.

[28] Sungho Jo. *Hierarchical neural control of human postural balance and bipedal walking in sagittal plane.* PhD thesis, MIT, 2007.

[29] M.P. Kadaba, H.K. Ramakrishnan, E. Wootten, J. Gainey, G. Gorton, and G.V.B. Cochran. Repeatability of kinematic, kinetic, and electromyographic data in normal adult gait. *J. Orthop. Res.*, 7:pp.849–860, 1989.

[30] M.P. Kadaba, H.K. Ramakrishnan, and M.E. Wootten. Measurement of lower extremity kinematics during level walking. *J. Orthop. Res.*, 8:pp.383–392, 1990.

[31] K.Deb and T. Goel. Controlled elitist non-dominated sorting genetic algorithms for better convergence. In *International conference on evolutionary multi-criterion optimization ()EMO-2001)*, pages pp.67–81, 2001.

[32] D.Casey Kerrigan, Ugo Della Croce, Michael Marciello, and Patrick O. Riley. A refined view of the determinants of gait: Significance of heel rise. *Archives of Physical Medicine and Rehabilitation*, 81(8):pp.1077–1080, 2000.

[33] D.Casey Kerrigan, Patrick O. Riley, Jennifer L. Lelas, and Ugo Della Croce. Quantification of pelvic rotation as a determinant of gait. *Arch. Phys. Med. Rehab*, 82:pp.217–220, 2001.

[34] S. P. Ma and G. I. Zahalak. A distribution-moment model of energetics in skeletal muscle. *Journal of Biomechanics*, 24:pp.21–35, 1991.

[35] C. MacKinnon and D. Winter. Control of whole body balance in the frontal plane during human walking. *J Biomech.*, 26(6):pp.633–44, 1993.

[36] S. Peter Magnusson, Nina Beyer, Heidi Abrahamsen, Per Aagaard, Kirsten Neergaard, and Michael Kjaer. Increased cross-sectional area and reduced tensile stress of the achilles tendon in elderly compared with young women. *Journal of Gerontology: BIOLOGICAL SCIENCES*, 58A(2):pp.123–127, 2003.

[37] T. Mcgeer. Passive dynamic walking. *International Journal of robotics research*, 9(2):pp.62–82, 1990.

[38] T. Mergner, C.Maurer, and R. J. Peterka. A multisensory posture control model of human upright stance. *Prog. Brain Res,*, 142:pp.189–201, 2003.

[39] Hanns Ruder Michael Gunther. Synthesis of two-dimentional human walking: a test of the lambda-model. *Bio. Cybern.*, 89:pp.89–106, 2003.

[40] H. Naito, T. Inoue, K. Hase, T. Matsumoto, and M. Tanaka M. Development of hip disarticulation prostheses using a simulator based on neuro-musculo-skeletal human walking model. *J. Biomechanics Abstract of the 5th World Congress of Biomechanics-*, 39, 2006.

[41] Richard R. Neptune, Craig P. McGowan, and Steven A. Kautz. Forward dynamics simulations provide insight into muscle mechanical work during human locomotion. *Exercise and Sport Science Reviews*, 37:pp.203–210, 2009.

[42] Richard R. Neptune, Kotaro Sasaki, and Steven A. Kautz. The effect of walking speed on muscle function and mechanical energetics. *Gait and Posture*, 28(1):pp.135–43, 2008.

[43] Naomichi Ogihara and Nomutoshi Yamazaki. Generation of human biped locomotion by a bio-mimetic neuro-musculo-skeletal model. *Biol. Cybern.*, 84:pp.1–11, 2001.

[44] S. M. OConnor and A. D. Kuo. Direction dependent control of balance during walking and standing. *J. Neurophysiol.*, 102:pp.1411–1419, 2009.

[45] P. Pkrishnawamy. A computational framework to study neural-structural interactions in human walking. Master's thesis, Massachusetts Institute of Technology, 2010.

[46] G.A. Pratt and M.W. Williamson MW. Series elastic actuators. *Proceedings on IEEE/RSJ International Conference on Intelligent Robots and Systems*, pages pp.399–406, 1995.

[47] Arthur Prochazka, Deborah Gillard, and David J. Bennett. Positive force feedback control of muscles. *J Neurophysiol*, 77:pp.3226–3236, 1997.

[48] H J Ralston. *Neural Control of Locomotion*, chapter Energetics of Human Walking, pages pp.399–406. Plenum Press, 1976.

[49] J. E. Butler R.D. Herbert, A. M. Moseley and S. C. Gandevia. Change in length of relaxed muscle fascicle3s and tendonswith knee and ankle movement in human. *Journal of Physiology*, 539:pp.637–645, 2002.

[50] RichardR.Neptune, DavidJ.Clark, and StevenA.Kautz. Modular controlofhumanwalking:asimulationstudy. *JournalofBiomechanics*, 42:pp.1282–1287, 2009.

[51] Seungmoon Song and Hartmut Geyer. Regulating speed and generating large speed transitions in neuromuscular human walking model. *IEEE International Conference on Robotics and Automation*, 2012.

[52] S Standring. *Gray's Anatomy.* Elsevier, 2008.

[53] G Taga. A model of the neuro-musculo-skeletal system for human locomotion i. emergence of basic gait. *Biol Cybern*, 73:pp.638–644, 1995.

[54] G Taga. A model of the neuro-musculo-skeletal system for anticipatory adjustment of human locomotion during obstacle avoidance. *Biol Cybern*, 78:pp.9–17, 1998.

[55] Yasuo Kawakami Senshi Fukashiro Hiroaki Kanehisa Tetsuo Fukunaga, Keitaro Kubo and Constantinos N. Maganaris. In vivo behavior of human muscle tendon during walking. *Proc Biol Sci.*, 268:pp.229–233, 2001.

[56] Brian R. Umberger, Karin G. M. Gerritsen, and Philip E. Martin. A model of human muscle energy expenditure. *Computer Methods in Biomechanics and Biomedical Engineering*, 6(2):pp.99–111, 2003.

[57] Brian R. Umberger and Philip E. Martin. Mechanical power and efficiency of level walking with different stride rates. *The Journal of Experimental Biology*, 210:pp.3255–3265, 2007.

[58] Cornell University. 2009 disability status report united states, 2009.

[59] J. J. Visser, J. E. Hoogkamer, M. F. Bobbert, and P. A. Huijing. Length and moment arm of human leg muscles as a function of knee and hip-joint angles. *Eur J Appl Physiol*, 61:pp.453–460, 1990.

[60] P. A. Willems, G. A. Cavagna, and N.C. Heglund. External, internal and total work in human locomotion. *Journal of Experiment Biology*, 198:pp.379–393, 1995.

[61] David A. Winter. Biomechanical motor patterns in normal walking. *Journal of Motor Behavior*, 15(4):pp.302–330, 1983.

[62] GT Yamaguchi, AGU Sawa, DW Moran, M J Fessler, and J M Winters. A survey of human musculotendon actuator parameters. Technical report, Multiple muscle Systems Biomechanics and Movement Organization, 1990.

[63] Kathryn Ziegler-Graham, Ellen J. MacKenzie, Patti L. Ephraim, Thomas G. Travison, and Ron Brookmeyer. Estimating the prevalence of limb loss in the united states: 2005 to 2050. *Archives of Physical Medicine and Rehabilitation*, 89(3):pp.422–429, 2008.